Front. Chem. Sci. Eng. 2020, 14(2): 188–215
https://doi.org/10.1007/s11705-019-1872-6

REVIEW ARTICLE

Metal-organic framework-based CO_2 capture: from precise material design to high-efficiency membranes

Yujie Ban[1], Meng Zhao[1,2], Weishen Yang (✉)[1]

1 State Key Laboratory of Catalysis, Dalian Institute of Chemical Physics, Chinese Academy of Sciences, Dalian 116023, China
2 University of Chinese Academy of Sciences, Beijing 100049, China

Abstract A low-carbon economy calls for CO_2 capture technologies. Membrane separations represent an energy-efficient and environment-friendly process compared with distillations and solvent absorptions. Metal-organic frameworks (MOFs), as a novel type of porous materials, are being generated at a rapid and growing pace, which provide more opportunities for high-efficiency CO_2 capture. In this review, we illustrate a conceptional framework from material design and membrane separation application for CO_2 capture, and emphasize two importance themes, namely (i) design and modification of CO_2-philic MOF materials that targets secondary building units, pore structure, topology and hybridization and (ii) construction of crack-free membranes through chemical epitaxy growth of active building blocks, interfacial assembly, ultrathin two-dimensional nanosheet assembly and mixed-matrix integration strategies, which would give rise to the most promising membrane performances for CO_2 capture, and be expected to overcome the bottleneck of permeability-selectivity limitations.

Keywords CO_2 capture, CO_2-philic MOFs, crack-free membranes

1 Introduction

Traditional energy structures overly relying on fossil fuels cause a large global emissions of CO_2 as one of the prime contribution to global warming, which has long remained a topical issue in research and industry. In high-latitude regions of Earth, temperatures have risen twice as fast as the global average [1]. CO_2 capture and storage is one of the most promising methods to mitigate global warming and other consequent environment problems. In particular, a growing interest has appeared in post-combustion CO_2 capture and pre-combustion CO_2 capture, which is always concomitant with two challenging processes, namely CO_2/N_2 separation and H_2/CO_2 separation. CO_2 is an undesirable component in natural gas, lowers the energy content of CH_4 and causes pipeline corrosion in the presence of moisture. CO_2 sequestration from natural gas is a challenging option with great significance to methane upgrading and the environment. CO_2 capture issues, which typically refer to the splitting of CO_2/N_2, H_2/CO_2 and CO_2/CH_4, have drawn considerable interest, and have been studied extensively based on amine scrubbing, ionic-liquid absorbtion and molecular-sieve adsorption [2–4].

Metal-organic frameworks (MOFs), as an important class of molecular sieves, are built from organic linkers and inorganic metal (or metal-containing cluster) nodes and embody renowned series, for example, metal azolate frameworks (MAFs) [5], zeolite imidazole frameworks (ZIFs) [6], Hong Kong University of Science and Technology (HKUST) [7], isoreticular metal-organic frameworks (IRMOFs) [8], Materials of Institute Lavoisier (MIL) [9], University of Oslo (UiO) [10], and Christian Albrechts University (CAU) [11]. MOFs have impressive features of ultra-porosity, diversified chemical compositions and designable porous architecture, which provide them with great potential for CO_2 capture.

Membrane separations based MOFs are anticipated to significantly reduce energy consumption compared with traditional distillation and yield opportunities for CO_2 capture [12]. A huge obstacle is the construction of desirable MOF membranes with a high permeability and selectivity. If we consider the adsorption-diffusion transportation model of MOF membranes, the improvement in separation performances can be achieved by optimizing the adsorption and diffusion properties. Two essential themes should be considered: (i) design and modification of CO_2-philic MOF materials and (ii) construction of crack-free

Received March 31, 2019; accepted May 30, 2019

E-mail: yangws@dicp.ac.cn

membranes. Material design and modification is indispensable for gaining desirable membrane materials because MOF chemical/structural features jointly determine their selective adsorption and molecular transportation properties. Metal ions and organic linkers as fundamental building units comprise the entire MOF skeleton through coordination bonds, and provide selective binding sites for CO_2 with assignable contributions of chemical interaction. Structural factors, such as the pore shape, size, flexibility and topology assortment, determine the accessibility of MOFs to CO_2 and other competitive guest molecules (adsorbed or excluded) and influence the transportation properties of MOFs. Meanwhile, it is critical to explore the synthesis technologies for crack-free MOF membranes, which will eliminate the negative effect of crack flow and fully exploit the chemical/structural features of MOF materials for membrane-based CO_2 capture.

In this review, we illustrate a conceptional framework from material design to separation applications for CO_2 capture (Fig. 1) and emphasize two important themes, namely (i) design and modification of CO_2-philic MOF materials and (ii) construction of crack-free membranes, which would yield the most promising membrane performances for CO_2 capture and be expected to overcome the bottleneck of permeability-selectivity limitations.

2 Target-oriented design and modification of CO_2-philic MOF materials

CO_2-philicity of MOFs implies a well-matched host-guest relationship between MOFs and CO_2 molecules, and gives rise to ideal selective adsorption and facilitates transportation properties for CO_2 capture. Material design and modification is indispensable for gaining desirable membrane materials because chemical/structural features of MOFs jointly determine the selective adsorption and molecular transportation properties. Accordingly, a rational series of pre- and post-synthetic approaches is targeted at secondary building units, pore structure, topology and hybridization for achieving CO_2-philic MOF materials.

2.1 Secondary building units

MOFs, by definition, are established by two kinds of secondary building units (SBUs), namely metal-containing SBUs and organic linker SBUs, which provide anchor

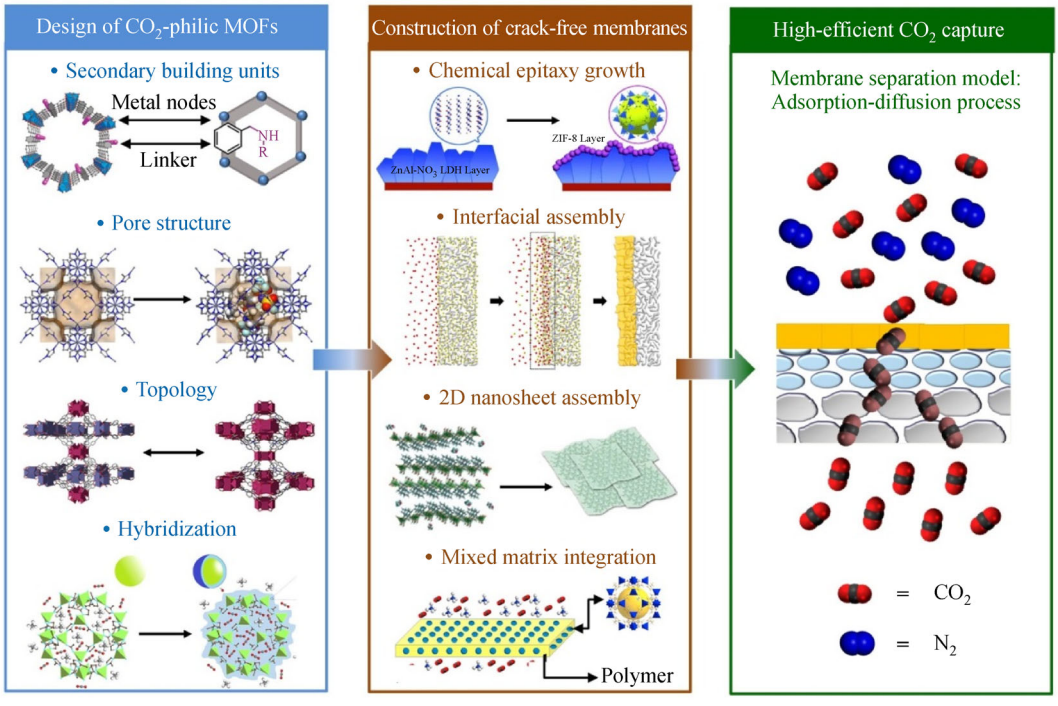

Fig. 1 Illustration of the conceptional framework from material design and separation application for CO_2 capture, involving strategies towards design of CO_2-philic MOFs and construction of crack-free membranes to achieve high-efficient CO_2 capture. The images in the first column from top to bottom: reproduced with permission [13], copyright 2014, American Chemical Society; reproduced with permission [14], copyright 2015, Wiley-VCH; reproduced with permission [15], copyright 2015, American Chemical Society; reproduced with permission [16], copyright 2018, American Chemical Society. The images in the second column from top to bottom: reproduced with permission [17], copyright 2015, Wiley-VCH; reproduced with permission [18], copyright 2018, American Chemical Society; reproduced with permission [19], copyright 2017, Wiley-VCH; reproduced with permission [20], copyright 2018, Elsevier.

points for CO_2 molecules and are associated closely with CO_2 selective adsorption. If we consider the chemical flexibility of these two types of SBUs, the design and modification of SBUs of MOF materials via synthetic MOF chemistry has been expected to yield CO_2-philic materials and further improve the CO_2-sorption benchmark.

2.1.1 Metal-containing SBUs

Open metal sites with coordination vacancies often bear partial positive charges, and have been evidenced experimentally to act as preferential adsorption sites for CO_2 with a large quadrupole moment and polarizability [21–26]. Based on first-principle calculations, the adsorbed CO_2 molecule is attached to the metal sites via an end-on orientation mode through one of its closest oxygen atoms, whereas the remaining atoms are orientationally free. The significant electrostatic interaction between MOFs with open metal sites and CO_2 molecules drives selective CO_2 sequestration and separation from other gas molecules, such as N_2 and CH_4, as exemplified by HKUST-1 and MOF-74 (CPO-27) [26,27]. As shown in Table 1, Mg-MOF-74 exhibited the highest CO_2 capacity among the MOF-74 series by experiment. The distinguished adsorption performance arises from the formation of semi-ionic Mg (MOF-74)-O (CO_2) bonds [27]. By using density functional theory (DFT) calculations, Jung and co-workers proposed that MOF-74 can be tuned to have a stronger binding affinity for CO_2 by metal substitution. For V and Ti-MOF-74, the interaction of lone-pair orbitals of CO_2 with the empty metal d-levels can be interpreted as coordination bond interaction, which is conductive to a higher binding energy for CO_2 compared with Mg-MOF-74 by 6–9 $kJ \cdot mol^{-1}$ (Table 1) [28].

Heterometallic MOFs with integrations of chemically dissimilar metal ions have been expected theoretically to create variations in properties and provide synergistic binding sites for CO_2. As proof-of-concept, Zhai et al. systematically designed a series of MOFs consisting of trivalent metals (M_1^{3+}) and divalent metals (M_2^{2+}) that occupied crystallographically equivalent sites (denoted CPM-200-M_1/M_2), which provided opportunities to alter the gas sorption properties of the MOFs (Fig. 2). Among the diversified metal ion combinations in the same MOF platform, CPM-200-Fe/Mg exhibited a remarkable CO_2 adsorption, and reached 5.68 $mmol \cdot g^{-1}$ at 298 K and 1 bar (Table 1). CPM-200-V/Mg offered a chemospecific affinity to CO_2 as a result of π back-bonding by V^{3+}. The adsorption heat of CPM-200-V/Mg for CO_2 reached up to 79.6 $kJ \cdot mol^{-1}$, which is much higher than that of the other MOFs (Table 1) [29].

In view of the examples above, we can distinguish the power of MOFs with open metal sites as CO_2 scavengers. Simultaneously, we should assess the influence of charge, radius, density and valence electron structure of central metal ions and the cavity size of the resultant framework on CO_2 adsorption, which is associated closely with the type of interaction and binding orientation. The strong CO_2 affinity to open metal sites will improve the MOF adsorption heat, which proves an obstacle for MOF desorption and recycling, but is still desirable for high-temperature post-combustion CO_2 capture. A significant challenge in material design is to garner catenated and ordered frameworks by combining unusual metal ions with linkers through crystallization. The post-synthetic metal

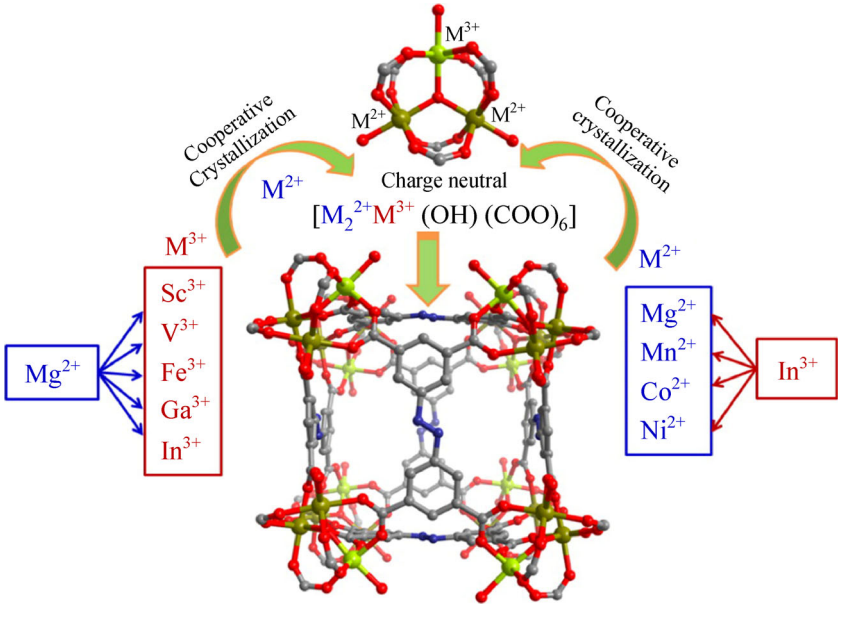

Fig. 2 M^{2+} and M^{3+} combinations for CPM-200 [29]. Copyright 2016, American Chemical Society.

Table 1 CO_2 adsorption capacity, heat and selectivity of typical MOFs

MOFs	CO_2 uptake capacity/ ($mmol \cdot g^{-1}$)	Condition	Q_{st}/($kJ \cdot mol^{-1}$)	CO_2/CH_4	CO_2/N_2	Method	Ref.
HKUST-1	4.44	295 K, 1 bar	–	5.5	20.2	Henry's law	[26]
Mg-MOF-74	8.0	296 K, 1 bar	47 (41.4)[a)]	–	–	–	[27,28]
Co-MOF-74	7.0	296 K, 1 bar	37	–	–	–	[27]
Zn-MOF-74	5.1	296 K, 1 bar	–	–	–	–	[27]
Ni-MOF-74	5.8	296 K, 1 bar	41	–	–	–	[27]
Ti-MOF-74	–	–	(50.1)[a)]	–	–	–	[28]
V-MOF-74	–	–	(47.3)[a)]	–	–	–	[28]
CPM-200-Fe/Mg	5.68	298 K, 1 bar	34.3	–	201 (50:50) (273 K)	IAST	[29]
CPM-200-V/Mg	3.59	298 K, 1 bar	79.6	–	406 (50:50) (273 K)	IAST	[29]
HHU-5	4.78	298 K, 1 bar	25.6	6.2 (20:80)[b)]	21.2 (20:80)[b)]	IAST	[39]
IFMC-1	2.7	298 K, 1 bar	30.7	–	26.9	Capacity ratio[c)]	[40]
Cu-TDPAT	5.89	298 K, 1 bar	42.2	–	79 (10:90)[b)]	IAST	[41]
bio-MOF-11	4.1	298 K, 1 bar	45	–	75	Henry's law	[45]
ZIF-78	2.7[d)]	298 K, 1 bar		10.6	50	Henry's law	[46]
ZIF-81	2.2[d)]	298 K, 1 bar		5.7	24	Henry's law	[46]
ZIF-79	1.6[d)]	298 K, 1 bar		5.4	23	Henry's law	[46]
ZIF-69	2.2[d)]	298 K, 1 bar		5.1	20	Henry's law	[46]
ZIF-68	1.7[d)]	298 K, 1 bar		5.0	18	Henry's law	[46]
ZIF-82	2.2[d)]	298 K, 1 bar		9.6	35	Henry's law	[46]
ZIF-70	1.1[d)]	298 K, 1 bar		5.2	17	Henry's law	[46]

a) Calculated by PBE-D2 method. b) Molar ratio of CO_2 to N_2 in a model mixture. c) Determined by the ratio of adsorbed amount of CO_2 at 0.15 bar to N_2 at 0.75 bar from isotherms. d) $mmol \cdot cm^{-3}$ as capacity unit.

exchange strategy has been demonstrated to be a supplement in material design, which overcomes the activation energy barrier for homogeneous nucleation of MOFs.

2.1.2 Organic linker SBUs

Organic linkers with nucleophilic groups provide sites for trapping CO_2 by Lewis acid-base interactions, exemplified with nitrogen-containing pyridine and azole which affect the gas uptake and selectivity of MOF materials significantly. Zhang and co-workers used nitrogen-rich azole linkers and synthesized a series of stable MAFs [30–36]. One of the most famous MAF materials is zeolite-analogous MAF-4 that was constructed by Zn^{2+} and 2-methylimidazole (also known as zeolitic imidazolate framework-8, ZIF-8) [37]. MAF materials possess a unique framework structure and active uncoordinated azolate nitrogen donors on the pore surface, which shows great potential in CO_2 response and selective adsorption. C_3-symmetric triazole-containing dendritic hexacarboxylate linker was designed and synthesized to achieve a nitrogen-rich rht-NTU-105. The experimental tests and theoretical molecular simulations demonstrated that the incorporation of coordination-free nitrogen-rich triazole moieties into struts of rht-type MOFs is an ideal choice to enhance the adsorption affinity towards CO_2 [38]. A similar phenomenon appeared in the Cu-carboxylic acid "paddle-wheel" based 3D structure HHU-5, which possesses a CO_2 uptake adsorption capacity of 4.78 $mmol \cdot g^{-1}$ at 298 K at 1 atm (Table 1), and is ascribed to free nitrogen atoms unbonded to copper ions in tetrazole ligands [39]. Qin et al. achieved a 3D zeolite-like MOF by the self-assembly of a stable N-rich organic azole linker and nontoxic metal ions, namely IFMC-1, [Zn(Hdttz)]·DMA (IFMC = Institute of Functional Material Chemistry; H_3dttz = 4,5-di(1H-tetrazol-5-yl)-2H-1,2,3-triazole; DMA = N,N′-dimethylacetamide). IFMC-1 possessed abundant uncoordinated nitrogen atoms from N-rich aromatic azole linkers, corresponding to ~63.6% of the N-donor sites being uncoordinated with Zn(II) in the structure, which would provide a new opportunity for the design and synthesis of CO_2-philic adsorbents in the future [40]. Triazine-containing functional linkers have a high N-donor site density, which may account for the strong binding affinity of CO_2 to MOF materials. For example, rht-MOF Cu-TDPAT $[Cu_3(TDPAT)(H_2O)_3] \cdot 10H_2O \cdot 5DMA$ (H_6TDPAT = 2,4,6-tris(3,5-dicarboxylphenylamino)1,3,5-triazine) was designed and synthesized based on a hexacarboxylate ligand with triazine backbone, and

showed a remarkable CO_2 adsorption capacity (5.89 mmol·g^{-1} at 298 K and 1.0 atm) and isosteric heat (42.2 kJ·mol^{-1}) compared with other isoreticular rht-MOFs [41].

Amine grafting has proven effective in increasing the uptake and selectivity of CO_2. Organic linkers that are functionalized with a range of aromatic, primary, secondary and tertiary amines were introduced to form an extended structure of IRMOF-74-III (IRMOF-74-III-CH_3, -NH_2, -CH_2NHBoc, -$CH_2NMeBoc$, -CH_2NH_2 and-CH_2NHMe) and were tested for their CO_2 capture properties (Fig. 3). IRMOF-74-III-CH_2NH_2 and IRMOF-74-III-CH_2NHMe exhibited a strong affinity for CO_2 because they showed the highest uptake at an extremely low CO_2 pressure (<1 Torr; 1 Torr = 0.00133 atm) (Figs. 3(b) and 3(c)). Cross-polarization magic angle spinning ^{13}C NMR spectra confirmed that CO_2 bond chemically to aliphatic amine functionalities (-CH_2NH_2 and -CH_2NHMe) and carbamate species were generated. Interestingly, the CO_2 selective capture behavior of IRMOF-74-III-CH_2NH_2 from humid flue gas (16% of CO_2, 84% of N_2 and 65% of humidity) remains unchanged against that under dry flue gas (Fig. 3(d)), which underlines the practical utility of amine-functionalized MOFs in post-combustion CO_2 capture. Decorated amino groups frequently exhibit a synergistic effect with nitrogen-rich linkers, which leads to a striking enhancement of CO_2 capacity and selectivity [42]. Another typical example is Bio-MOFs that were established on adenine-based biomolecular building blocks, which expose accessible amino groups synergistically combined with available pyrimidine to interact with CO_2 [43,44]. For example, Bio-MOF-11 was designed and synthesized by the self-assembly of cobalt-adeninate-acetate "paddle-wheel" clusters. Owing to the synergistic effect of amino and pyrimidine groups of adenine, Bio-MOF-11 has a high heat of adsorption for CO_2 (45 kJ·mol^{-1}), a high CO_2 capacity (4.1 mmol·g^{-1} at 1 atm and 298 K) and an impressive selectivity for CO_2 over N_2 (75 at 298 K) [45]. Theoretically, the binding strength is proportional to the numbers of amino groups.

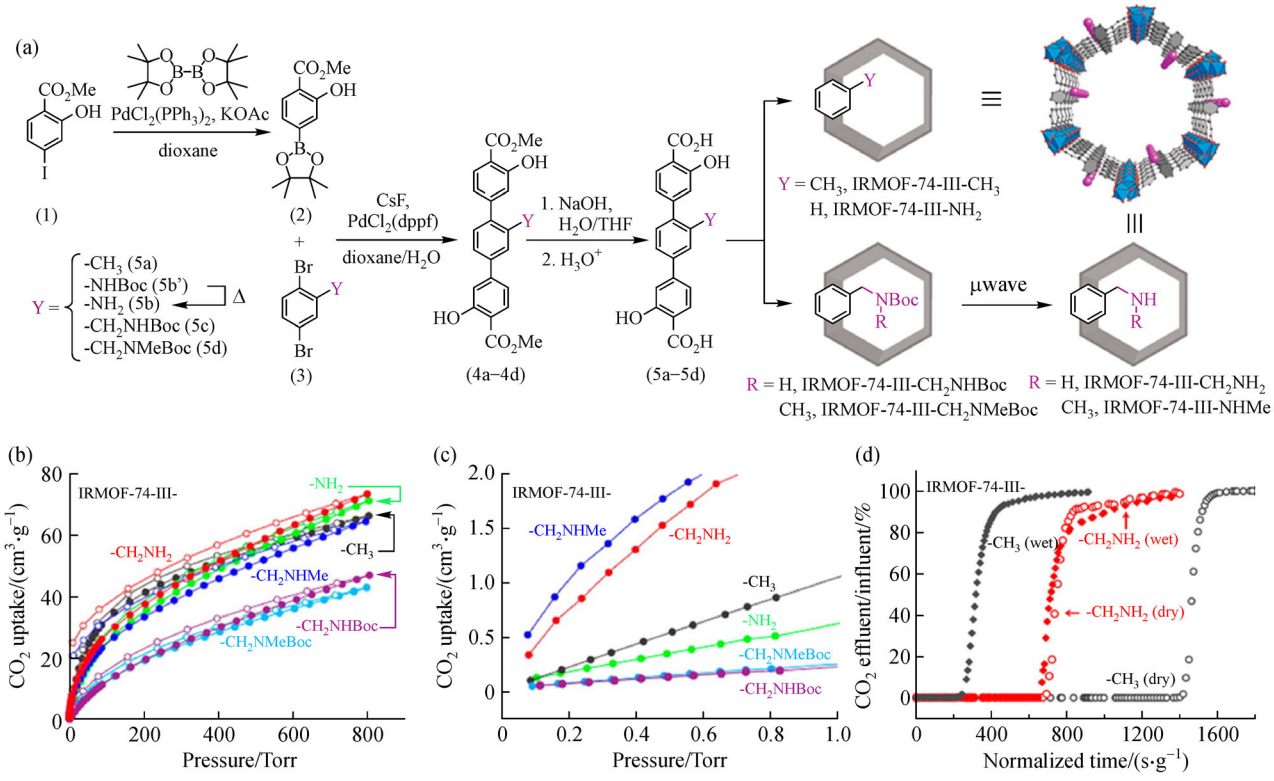

Fig. 3 (a) Synthetic pathway for the functionalized organic linkers used in the synthesis of IRMOF-74-III. This methodology allowed us to prepare -CH_3, -NH_2, -CH_2NHBoc and -$CH_2NMeBoc$ (5a–5d) functionalized linkers. On the right is shown a schematic representation of the IRMOF-74-III pore functionalized with the organic linkers 5a–5d and post-synthetic deprotection of Boc groups. Color code: C in gray, O in red, functional groups in purple, Mg as blue polyhedra. (b) Comparison of CO_2 uptake at 25°C for IRMOF-74-III-CH_3 (gray), -NH_2 (green), -CH_2NH_2 (red), -CH_2NHMe (blue), -CH_2NHBoc (purple), and -$H_2NMeBoc$ (cyan). (c) Expansion of the low pressure range (<1 Torr). CO_2 isotherms at 25°C for IRMOF-74-III-CH_2NH_2. (d) Breakthrough curves for IRMOF-74-III-CH_3 under dry conditions (gray empty markers) and wet conditions (gray filled markers), and for IRMOF-74-III-CH_2NH_2 under dry conditions (red empty markers) and in the presence of water (red filled markers). Reproduced with permission [13], copyright 2014, American Chemical Society.

Nevertheless, we should consider the steric effect and variation of the accessible pore volume resulting from the decoration of groups. The challenge in material design and modification is how to balance the physisorption (pore) and chemical binding (amino groups) to optimize the CO_2 capacity and selectivity, which is associated closely with the dynamic performances of MOF-based membrane separation.

Despite Lewis acid-base interactions, polar groups that were decorated on MOFs can drive the selective adsorption of CO_2 by taking advantage of dipole-quadrupole interactions with CO_2, which has a noticeable quadrupole moment. The validity of this concept can be confirmed by GME-type ZIFs that were designed by Yaghi and coworkers, wherein Zn^{2+} is connected tetrahedrally to two specific imidazolate linkers (2-nitroimidazolate) and two other substituted imidazolate linkers to make an isostructural three-dimensional topology net. The CO_2 binding affinity of ZIFs can be finely tuned by varying the substituted imidazolate linkers with diverse polar functionalities. As a result, the CO_2 capacity at 1 bar varied in the sequence ZIF-78 (-NO_2) > ZIF-82, -81, -69 (-CN, -Br, -Cl) > ZIF-68, -79 (-C_6H_6, -Me) > ZIF-70 (-H), which agrees with the order of dipole moments of the functionality and interaction between polar groups with CO_2 [46]. ZIF-78 has a high capacity for CO_2 (2.7 $mmol \cdot g^{-1}$ at 1 atm and 298 K) and a significant selectivity for CO_2 over N_2 (50 at 298 K) and CH_4 (10.6 at 298 K), and emerges as the best CO_2-selective ZIF adsorbent for post-combustion carbon capture and natural gas purification. Researchers also found that the favorable affinity for CO_2 arises in MOFs with a significant number of accessible hydroxyl group, which is exemplified by CD-MOF-2 that is composed of renewable γ-cyclodextrin and alkali metal ions. The free hydroxyl groups outside the γ-CD cavity trapped CO_2 with the formation of carbonic acid, as shown by the ^{13}C NMR spectroscopy [47]. This moderate and reversible interaction would help to facilitate dynamic transportation processes, and gain much attention in terms of a lower energy consumption.

Selective CO_2 sequestration occurring at the linker sites always shows successful sorption behavior in dry and humid conditions. This is a major advantage over MOFs that fix CO_2 only through metal-containing SBUs because the open metal sites would be occupied by water molecules and unavailable in moisture. The rational design and synthesis of MOFs has been facilitated significantly by computational methods of reticular chemistry and crystal engineering strategies at multi-scales [48], wherein metal-containing SBUs are connected by requisite organic linkers to permit *in situ* formation of ordered networks. Advances in MOF chemistry, in this regard, are highly dependent on linker design with a simultaneous consideration of their functionality and geometry and length. For MOF synthesis, predesigned linkers serve as structure directing agents (SDAs) to determine the metal-linker extension and the resultant framework net; the length and steric effect of linkers determine the accessible pore volume and interpenetration degree of MOFs, which is a factor that influences the adsorption properties of MOFs significantly. Open metal sites can cooperate with functional linkers for selective CO_2 adsorption, which improves the CO_2 specificity significantly and maintains optimal performances in dry and humid condition. Additionally, post-synthetic modification (PSM) has emerged as a powerful tool for tailoring the CO_2-philicity of MOFs without changing the underlying topology, which provides opportunities for incorporation of complexity within MOFs in a controlled manner. Two points are particularly important: (i) the incorporation of predesigned linkers into MOF matrices through linker substitution [49]; (ii) covalent grafting of CO_2-philic functionality into an MOF framework by click chemistry [50,51].

2.2 Pore structure

2.2.1 Aperture/cage

The pore structures of MOFs play a key role in CO_2 selective adsorption and transportation. MOFs with a large microporosity exhibit a remarkable CO_2 affinity. Cage-like MOFs with wide cavities and narrow aperture windows provide a well-matched host-guest relationship and exhibit a superior CO_2 trapping capacity in terms of the confinement effect. ZIFs, which are composed of transition metal ions and imidazolate linkers, represent a typical cage-like 3D framework that frequently resembles zeolite topologies, which have been demonstrated to be an ideal type of CO_2 capturer. Cage-based structures are also formed by the assembly of metal-containing SBUs and multicarboxylic acid linker units [52]. Yu et al. reported cage-based $\{[Ni_3(abtc)_{1.5}(tpt)(H_2O)_5(DMF)] \cdot (DMF)_3 \cdot (H_2O)_6\}_n$ (NUM-3) (H4abtc = 3,3′,5,5′-azobenzenetetracarboxylic acid, tpt = 2,4,6-tri(4-pyridinyl)-1,3,5-triazine). NUM-3 crystals were synthesized through a mixed-linker strategy, with N-donor triazines as main linkers and carboxylic acids as auxiliary linkers. In the NUM-3 framework, four different cage types, denoted A, B, C and D with an inner diameter of 13, 10, 7 and 4 Å, respectively, were arranged in the ABCDDCBA order along the *c* axis as the minimum repeat unit. NUM-3 with characteristics of a multi-cage structure exhibited a remarkable CO_2 specificity [53].

The aperture windows of cage-like MOF materials always perform as molecular gates, which allow the entry of small molecules and exclude bulky molecules. Tailoring of the cut-off aperture window size in the suitable range is an indispensable strategy to optimize adsorption selectivity and transportation properties of materials on the premise that the catenated cage-like structures are not decomposed. Cage size tuning has proven a feasible way to improve the CO_2 affinity. A typical example is the space partition

strategy [54–56], which refers to the division of a large cage space into smaller segments, forming a cage-within-a-cage structure in which the density of binding sites and the host-guest interactions could be enhanced (Fig. 4(a)). Space partition can take different forms, including rational framework interpenetration, which brings about significant CO_2 affinity and framework stability. This strategy can also extend to channel-like MOFs [55]. Space partition is a new method to design CO_2-philic pore structures and enhance molecular sieving properties. A significant challenge is to establish synergistic coordination modes between metal nodes and functional ligands as partial agents. In contrast with the space partial approaches mentioned above, the "cage occupying" concept appears as an easy-to-operate strategy to tailor the effective cage size and optimize the molecular sieving properties of cage-like MOF materials. As proof of concept, Yang and co-workers proposed that room temperature ionic liquid (RTIL) can be used as cage occupants to tailor the microenvironment of the MOF nanospace (Fig. 4(b)). The effective cage size of ZIF-8 was tailored to be between CO_2 and N_2 by confining bulky ionic liquids into the ZIF-8's nanocage. A significant improvement in CO_2/N_2 adsorption selectivity was achieved from 19 for ZIF-8 to 100 for ionic liquid-modified ZIF-8, which is among the best of CO_2-philic adsorbents [14]. This method highlights a new direction in the design of MOF materials for CO_2 specificity, as it tailors the suitable pore size for molecular sieving and enables a modification of the MOF nanospace with CO_2-philic segments.

2.2.2 Flexibility

The flexibility of the porous MOF structure is an unconventional characteristic compared with that of other porous inorganic materials. The dynamic structural behavior, such as breathing and gate-opening under some stimuli (e.g., temperature, pressure and guests), has great

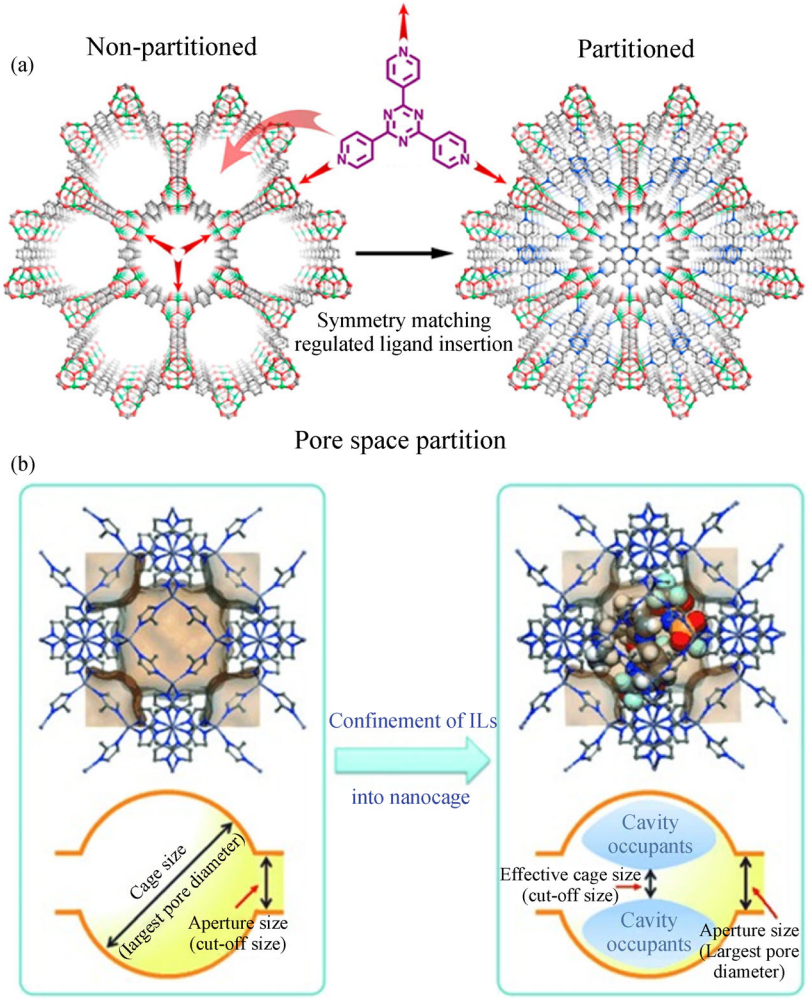

Fig. 4 (a) Illustration of pore space partition through symmetry matching regulated ligand insertion viewed along the *c* axis [56]. Copyright 2015, American Chemical Society. (b) Illustration of the cavity-occupying concept for tailoring the molecular sieving properties of ZIF-8 by incorporation of RTILs. The cut-off size shifts from the aperture size of six-membered ring to the reduced effective cage size by confinement of [bmim][Tf_2N] in a ZIF-8's SOD cage [14]. Copyright 2015, Wiley-VCH.

potential to trigger the selective adsorption of CO_2 [57]. Llewellyn and co-workers investigated the breathing phenomenon of flexible MIL-53, which led to different adsorption behaviors for CO_2 and CH_4 with pressure. Interestingly, a noticeable adsorption step was observed in CO_2 isotherms at ~5 atm along with a significant capacity at an extremely low pressure, which corresponds to the breathing effect of flexible MIL-53 networks. The CO_2 capacity improved consistently with an increase in pressure above 5 atm, which suggests a reopening of the total porosity and pore filling of materials [58]. The structural transitions of flexible MIL-53 upon adsorption of different gases were predicted further based on Osmotic Framework Adsorbed Solution Theory (OFAST), with the aim of selecting optimal operating conditions for CO_2 capture [59].

2.2.3 Meso/micro-hierarchical pores

Recently, MOFs with meso/micro-hierarchical pores have sparked substantial interest as a result of their superior gas uptake capacity and rapid mass transportation, which provides great potential for high efficiency CO_2 capture and separation [60–62]. Mao et al. designed and synthesized hierarchical porous HKUST-1 by using a ligand-assisted etching process [63]. The porous architecture of HKUST-1 crystals consisted of mesopores and micropores that were centered at 30 and 0.65 nm, respectively, and displayed a meso/micro-hierarchy. Interestingly, hierarchical HKUST-1 has a larger surface area (1462 $m^2 \cdot g^{-1}$ by BET estimation) than pristine crystals (1334 $m^2 \cdot g^{-1}$ by BET estimation), which leads to a notable enhancement in CO_2 capacity. The saturated time with CO_2 adsorption by hierarchical HKUST-1 was reduced from 10 to 5 min compared with pristine crystals, which means that meso/micro-hierarchical pores can change the adsorption kinetics significantly, and achieve rapid transportation of the loading equilibrium of target molecules. In general, the fabrication strategies towards MOFs with meso/micro-hierarchical pores involve topological designs, defect-doping, ligand-extension, etching, templating and other feasible methods [64]. The challenge for the synthesis of hierarchical MOFs is how to prevent excessive structure interpenetration and framework collapse during preparation and post-treatment procedures.

2.3 Topology

The topological structures of MOFs are expected to influence CO_2 adsorption and transportation properties critically. To make the best topological choice remains a permanent pursuit in the design of new MOFs for CO_2 capture. Reticular chemistry concepts have yielded new opportunities. Simultaneously, computational chemists contribute their wisdoms to the massive design and screening of optimal structural matrices to enable selective CO_2 physisorption. The multiscale approach, namely, the combination of molecular simulation and machine learning, proposed by Gómez-Gualdrón and co-workers, has been implemented to predict the role of various pore

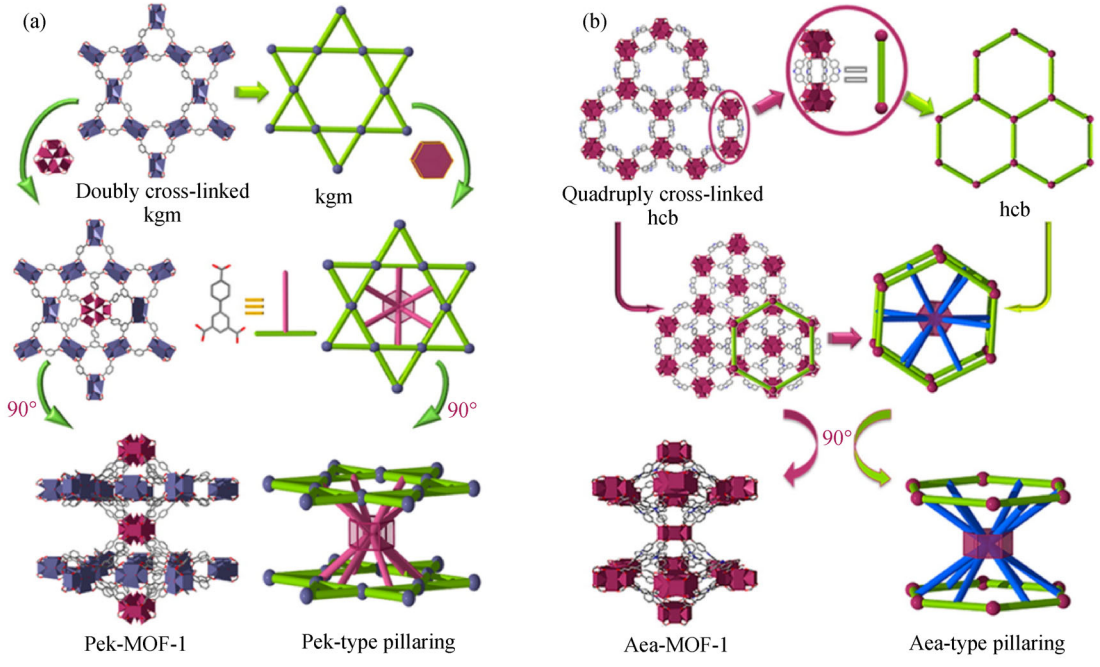

Fig. 5 (a) Schematic showing the new pek-type pillaring topology observed in pek-MOF-1; (b) schematic showing the aea-type pillaring topology observed in the aea-MOF-1 [15]. Copyright 2015, American Chemical Society.

chemistries and topological features, and emphasizes the importance of the topological structure on the CO_2 capture capabilities of MOFs [65].

For chemistry experimentalists, the molecular building block (MBB), the supermolecular building block (SBB), and the supermolecular building layer (SBL) approaches offer the potential to design MOFs with a specific topology where structural information can be included in the building blocks, and seal the gap from a computational prediction to the practice of reticular chemistry. Xue et al. have carried out systematic work. They demonstrated that bridging hexanuclear Re-based MBB clusters in a linear fashion through fluoro- or tetrazolate-functionalized organic linkers resulted in MOF formation with an fcu topology [66]. When linear linkers were replaced with quadrangular tetracarboxylate ligands, an ftw topology was obtained [67]. Given the parent topological structure, the carbon atoms of coordinated tetrazolate and carboxylate moieties act as points of extension and correspond to the formation of *iso*-reticular frameworks. The assortments of topological nets, in some cases, are also highly dependent on linker symmetry. A typical example is the construction of highly connected pek topological nets via a combination of Re metal salts with fewer symmetrical tricarboxylate linkers, which provide exceptional CO_2 capture properties (Fig. 5(a)) [15]. The use of another tricarboxylate ligand with contracted angles between the carboxylates from 120° to 90° led to a fascinating aea topological net (Fig. 5(b)). The pek-MOF and aea-MOF are also the first examples of pillar-based MOFs with a high pillar connectivity, which also proves the feasibility of the SBL approaches for the design and assembly of highly connected topological networks.

2.4 Hybridization

The chemical flexibility of MOFs has permitted their assembly and integration with other functional CO_2-philic materials (such as ionic liquids, amines and CNTs) to form highly compatible hybrids by mutual physical or chemical interactions. The hybridization can be implemented in three representative modes, i.e., cavity occupation and confinement, surface coating and chemical grafting.

2.4.1 Cavity occupation and confinement

Confinement of room temperature ionic liquids into the ZIF-8 nanocage represents a typical example of ionic liquid@MOF hybrids [14]. The ionic liquid, 1-butyl-3-methylimidazolium bis(trifluoromethyl-sulfonyl) imide ([bmim][Tf_2N]), as the second integration phase was a smart choice because the anion moiety favors CO_2 adsorption and the cation moiety is sufficiently bulky for efficient cavity occupancy, and achieves an effective alteration of the molecular sieving properties of ZIF-8 (Fig. 4(b)). Significant improvement in CO_2/N_2 and CO_2/CH_4 adsorption selectivity was obtained. Another example is amine@MOF hybrids. Inspired by amine scrubbing process, Zhong et al. reported a double-solvent incorporation strategy to inject the molecule-level organic amines, namely tris (2-aminoethyl) amine (TAEA), ethylenediamine (ED) and triethylene diamine (TEDA), separately into MIL-101(Cr) cavities under the action of capillary force (Fig. 6). The strong intermolecular interactions between amines and CO_2 led to a notably improved affinity of modified materials to CO_2, in particular for TAEA@MIL-101 (Cr) with 1.5 times of CO_2 uptake as

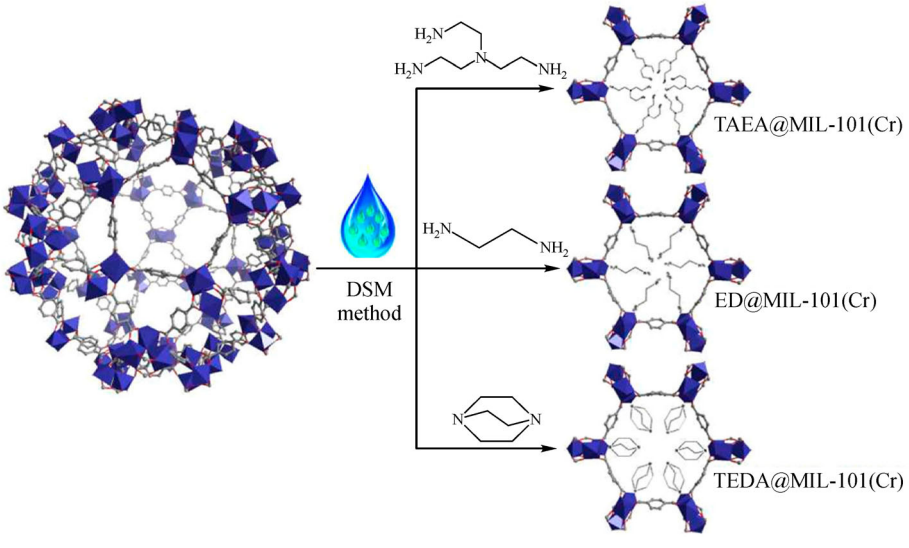

Fig. 6 Schematic diagram of grafting MIL-101(Cr) with three different amines [68]. Copyright 2018, American Chemical Society.

high as that of unmodified MIL-101(Cr) and a superhigh adsorption heat [68]. The pore blockage of amine molecules can reduce the material pore size effectively. The molecular sieving effect can be enhanced, which corresponds to an enhancement of CO_2/CO adsorption selectivity of amine-impregnated MOF materials. Lin et al. confined polyamine into the pores of MIL-101(Cr), which improved the selective CO_2 adsorption capacity significantly at a low pressure and ambient temperature. The influence of the molecular weight of PEI (polyetherimide) was assessed on the gas sorption properties of hybrids [69].

2.4.2 Surface coating

Zeeshan et al. demonstrated another category of MOF-based hybrid materials, by decorating an ultrathin nanometer coating of hydrophilic ionic liquid, 1-(2-hydroxyethyl)-3methylimidazolium dicyanamide ([HEMIM][DCA]), onto the hydrophobic surface of ZIF-8 to form a controllable core-shell structure (Figs. 7(a) and 7(b)) [16]. Because of the opposite hydrophilic/hydrophobic characteristics, ionic liquid deposited only on the external MOF surface instead of penetrating into the pore openings, which allowed for the fine tuning of the selective transport of CO_2 and CH_4 molecules. Ionic liquid/MOF, as an unprecedented match pair, improved the CO_2/CH_4 adsorption selectivity significantly (Fig. 7(c)), which suggests that this simple and elegant modification strategy can be extended to design assortments of hybrids for high-efficiency CO_2 capture.

2.4.3 Chemical grafting

Chemical grafting has proven to be a feasible hybridization process in which the generation of chemical bonds guarantees the confirmed binding of heterogeneous phases. Kumar et al. proposed a hybridization strategy involving two steps (Fig. 8). Firstly, the graphene basal plane was

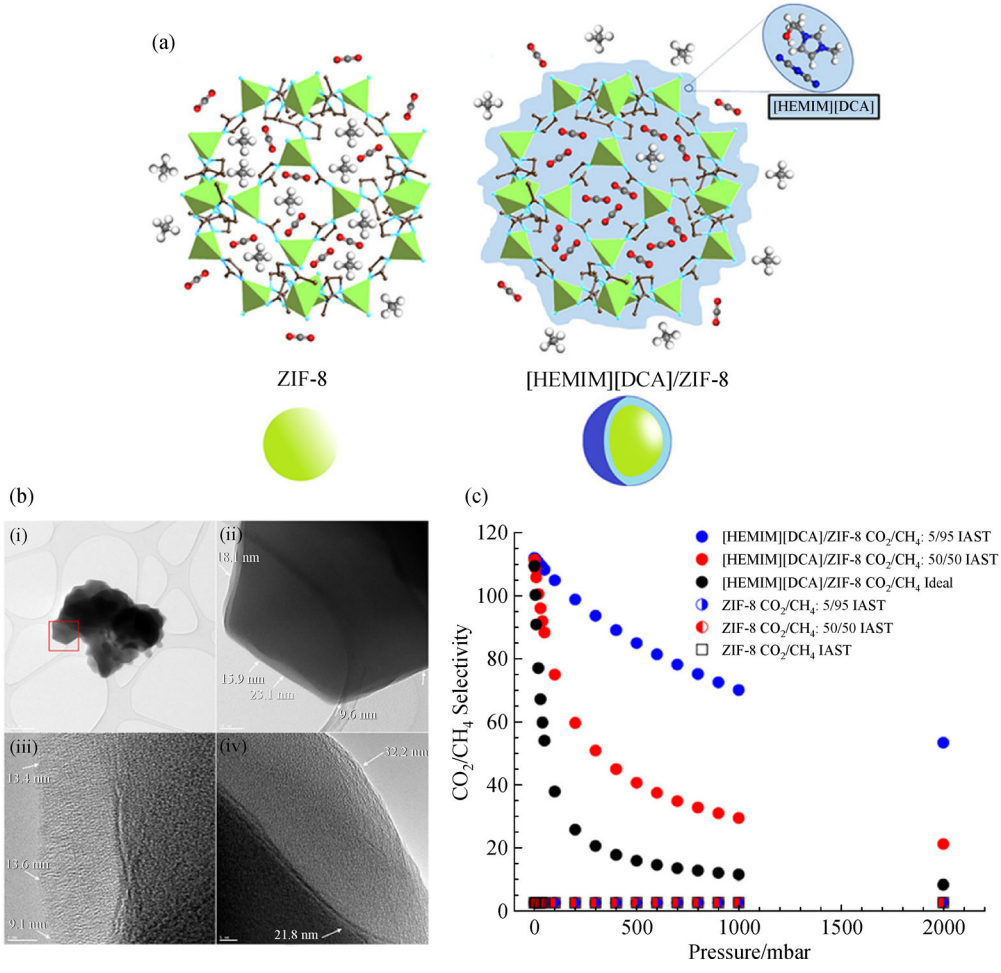

Fig. 7 (a) Proposed core–shell type [HEMIM][DCA]/ZIF-8 structure; (b) TEM images of [HEMIM][DCA]/ZIF-8 composite. Region in red-box in panel (i) is magnified in panel (ii). Panels (iii) and (iv) present higher magnification images at different locations focusing on the IL shell, respectively, where numbers on images represent the corresponding IL shell thickness at that location. (c) Ideal adsorption selectivity and IAST-predicted selectivities of ZIF-8 and [HEMIM][DCA]/ZIF-8 composite at room temperature. Reproduced with permission [16], copyright 2018, American Chemical Society.

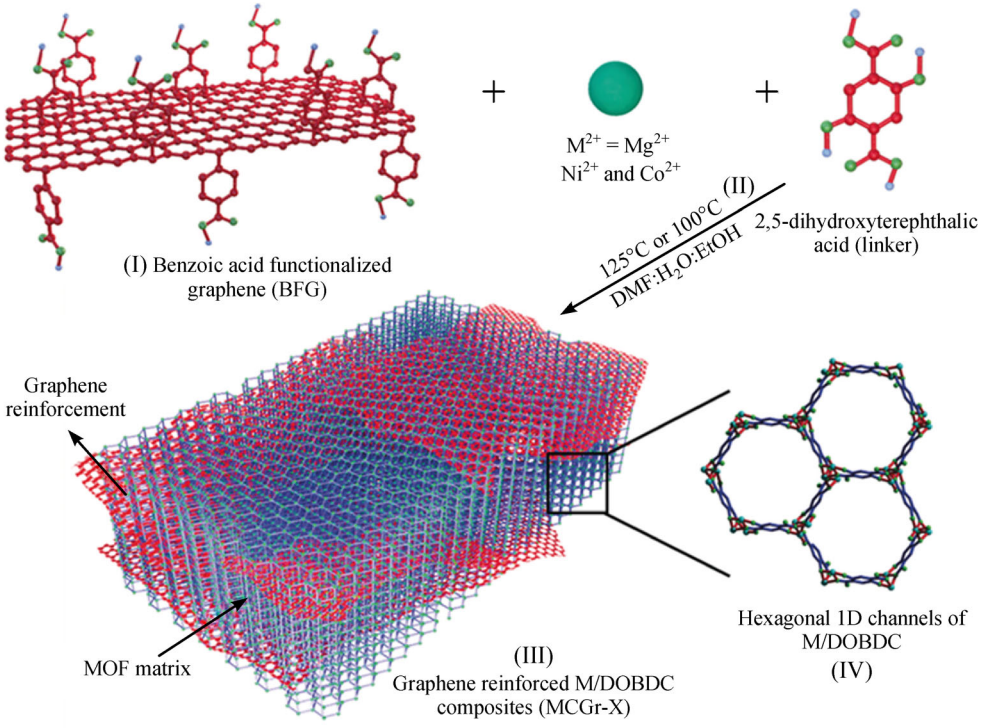

Fig. 8 Schematic representation of the synthesis of covalently linked grapheme/MOF composites [70]. Copyright 2016, Wiley-VCH.

functionalized by benzoic acid, and then benzoic acid as bridging linkers coordinated with metal ions. The graphene basal planes with reinforced frameworks were concomitant with the *in situ* growth of hexagonal one-dimensional (1D) channel-like MOF crystals, which were grafted covalently and firmly with the MOF matrix. The hybrids manifested a significantly higher surface area and an enhanced CO_2 adsorption capability, which is an intriguing result that involved the substantially improved mechanical properties of hybridization composites. A three-fold increase in the elastic modulus and hardness appeared with 5 wt-% graphene hybridization, which underlies the importance of graphene reinforcement for MOF crystals [70]. This concept paves the way for the design of MOF-based composite materials with a combination of improved gas sorption capacities and exceptional mechanical properties.

The exceptional chemical tunability makes MOFs compatible with many materials via multiple physical or chemical interactions, which allows for the generation of ideal hybrid and composite types. What excites experimentalists is the synergistic effect of hybrids, which shows contributions of $1 + 1 > 2$ to CO_2 adsorption specificity and other amazing physical properties. We stress the significance of the interfacial hybrid structure to gas transportation. Composite materials with carefully designed interphase hybridization structures will be needed, which facilitates CO_2 transportation and hinders other gases, such as H_2, N_2 and CH_4. MOF/MOF composites deserve special attention in which the growth of one MOF crystal on the surface of another MOF crystal is facilitated by taking advantage of the metal nodes or linkers as active grafting sites. Ban et al. proposed Ni/Zn-ZIF-108 and Co/Zn-ZIF-108 hybrids via controllable processes where Ni^{2+} or Co^{2+} substituted Zn^{2+} on the surface of parent ZIF-108 crystals and grafted into frameworks through coordination bonds without any destruction of the parent frameworks. Consequently, a core-shell mixed metal structure formed (Fig. 9(a)), which exhibited an improved CO_2 affinity [71]. Conversely, Cu^{2+} substitution occurred throughout the particles with the formation of homogeneous mixed metal ZIF materials (Fig. 9(b)). Analogous with MOFs, covalent organic frameworks (COFs) possess porous organic cages and well-defined topologies. MOF/COF hybrids were designed and constructed by integration of MOFs and COFs by covalently bonding reactions [72–75], which is promising in separation and other fields such as heterogeneous catalysis and photocatalysis. We assume that the special mixed phase composites would generate interest in the future by hybridization by a specific portion of one MOF (or COF, or other CO_2-philic materials) with the molecular sieving porous structure of another MOF, which may give rise to unprecedented performances in CO_2 selective adsorption and capture. MOF-based hybrids will yield new opportunities for CO_2 capture, which relies on highly controllable hybridization strategies from the molecular to the micro/nanometer level and advanced characterization methods.

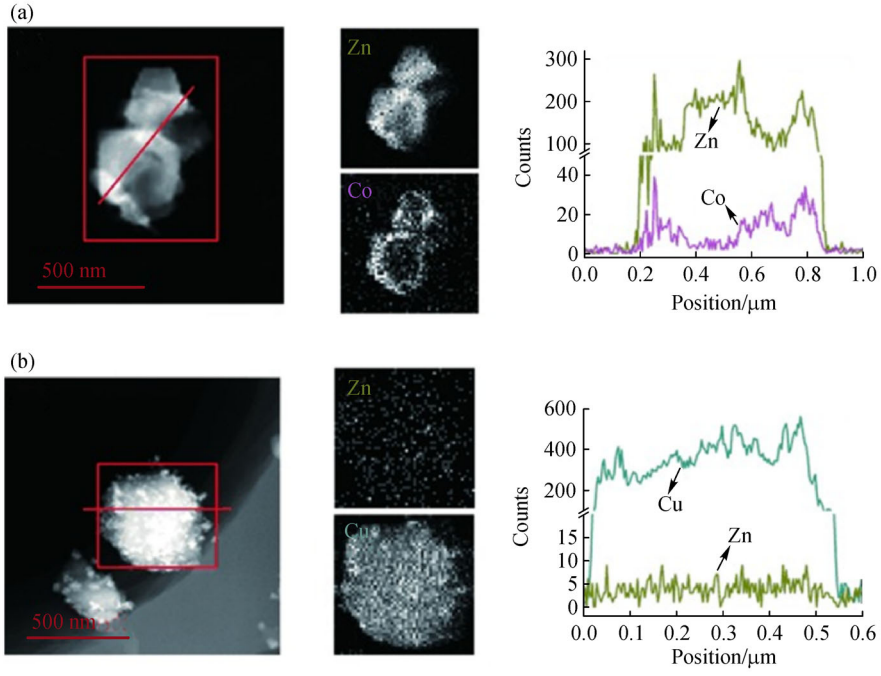

Fig. 9 HRTEM/EDX analysis of the mixed-metal materials Co-ZIF-108 (a) and Cu-ZIF-108 (b) [71]. Copyright 2014, Wiley-VCH.

3 Computational simulations of MOF membrane materials

With the growing computational power, molecular simulations play a critical role in materials science. Grand Canonical Monte Carlo (GCMC) and molecular dynamics (MD) simulations are computationally challenging but powerful to calculate the interactions between adsorbate-adsorbate and adsorbate-MOF and interpret the mechanism of adsorption separation. Zhang and co-workers simulated quasi-discrete pores that can induce conformational changes in the flexible guest molecules, which proved the essence of unprecedented adsorption separation performacnes of MOFs [76]. They also revealed the importance of hyperfine adjustment of flexible pore-surface pockets of MOFs by virtue of computational simulations, which can smartly control the accessibility of gas molecules with distinct molecular sizes and quadruple moments to the strongest adsorption sites [77].

Considering the large number of possible metal nodes and organic linkers and various combination ways, the number of MOFs is almost unlimited. Molecular simulations, accordingly, have been demonstrated to be an excellent tool to high-throughput screen ideal MOF membrane materials for CO_2 capture. Computational screening studies based on GCMC simulations generally focus on gas adsorption in MOFs. In the case of MOF membranes, gas diffusivities in the MOFs' pores should be calculated simultaneously by using equilibrium MD simulations. Computer-aided molecular simulations were initially performed to calculate adsorption constants (S_0) and self-diffusivities (D_0) of CO_2 and other gas molecules at infinite dilution. Gas permeabilities of MOF membrane were determined by using $P_0 = S_0 \times D_0$. The studies on screening MOF membranes for CO_2 capture mainly focused on assessing selectivity and permeability of a MOF membrane. The aim is to clarify the interplay of adsorptive and diffusive properties that drive the membrane-based separation. Keskin and co-workers used a multilevel, high-throughput computational screening methodology based on MOF database for membrane-based CO_2/CH_4 separation [78]. They found that MOFs that have a strong preference for CO_2 could favor CO_2 diffusion and dominated CO_2/CH_4 diffusion selectivity, resulting in a surprisingly higher membrane selectivity than adsorption selectivity. Qiao et al. corelated the CO_2 diffusion selectivity and adsorption selectivity with two structural parameters, namely the pore limiting diameter (PLD) and largest cage diameter (LCD), respectively, by using multilevel computational study to high-throughput screen 137953 MOFs for membrane separation of a $CO_2/N_2/CH_4$ mixture [79]. They revealed that MOFs with moderate percentage of PLDs located in a narrow range close to the kinetic diameter of CO_2 molecules were in favor of the improvement of CO_2 diffusion selectivity. The adsorption selectivity was high at the small PLD. It can be anticipated because the interaction between CO_2 and MOFs can be strengthened in the contracted nanospace. The high-throughput computational approach based on molecular simulations was popular for screening large

numbers of MOFs for membrane-based CO_2 capture and separation, where both of the high adsorption selectivity and diffusion selectivity were desirable [78–80]. However, it depends on a large amount of material sources and is time-consuming. By contrast, *in silico* discovery of high-performing membrane materials by applying a genetic algorithm (GA) can efficiently search a large database of MOFs for top candidates [81]. Metal nodes or linkers were substituted into the corresponding "parent MOFs" to generate "MOF children", which likewise evolved to create a subsequent generation. GA could be used to efficiently identify top-performing MOF membrane materials among thousands of hypothetical MOFs, which reduced the computational time by at least two orders of magnitude relative to a brute force search.

4 Construction of crack-free MOF membranes

It is critical to explore synthesis technologies for crack-free MOF membranes based on material design, modification and screening. Large cracks appear frequently at grain boundaries and grain-support interfaces. Owing to their negligible resistance, CO_2 and other target molecules penetrate through defects preferentially, and compromise the selectivity of the MOF membranes. Desirable membrane technologies and interfacial intensification approaches will help to eliminate the negative effect of crack flow, and take full advantages of the chemical/structural features of MOF membrane materials for CO_2 capture. Typical crack-free MOF membrane technologies are summarized and presented in the following text.

4.1 Chemical epitaxy growth of active building blocks

It has been proved feasible to construct MOF membranes from the chemical epitaxy growth of active building blocks (ABBs). Herein, multiscale ABBs, namely atomic/molecular-, nanometer- and micrometer-level ABBs are indispensable to crack-free membranes by virtue of their chemical reactivity and regrowth capability.

4.1.1 Atomic/molecular-level ABBs

Metal atoms/ions from substrates, as representative examples of atomic/molecular-level ABBs, are implemented frequently as active metal nodes to bond coordinatedly with organic linkers to facilitate *in situ* growth of continuous and crack-free MOF membranes. Guo et al. reported a "twin copper source" method in which active Cu points from copper net coupling with Cu^{2+} from the bulk synthesis solution provided metal sources for MOF crystallization, which contributed to the formation of continuous and compact $Cu_3(BTC)_2$ membranes [82]. Kang et al. chose a nickel screen as a membrane substrate and nickel metal precursor to fabricate Ni-based MOF membranes. During synthesis, the nickel screen was dipped into a linker solution that was composed of L-aspartic acid (L-asp) and 4,4′-bipyridine/pyrazine [83]. A thin layer of intergrown crystals appeared with the coordination reaction between the metal source and linkers, which played a key role in the subsequent synthesis of crack-free membranes (Fig. 10). Similarly, alumina substrates can also serve as a metal source to fabricate MIL-series membranes with Al as metal nodes [84]. Metal-based atomic/molecular-level ABBs from substrates as active sites of epitaxy growth promote membrane formation and strengthen the adherence between membrane and substrate. In addition to metal atoms/ions from substrates, diversified ultrathin metal films can also be deposited on substrates to providie atomic/molecular-level ABBs for MOF membrane fabrication with different metal nodes [85]. The functional linker assembly on the substrate surface is also considered as ABBs, which can bind metal ion precursors in solution for epitaxy growth [86–90]. An intriguing phenomenon is that the limited numbers of atomic/molecular-level ABBs from substrates potentially favor formation of ultrathin crack-free membrane with orientation, which relies on the precise control of parameters of epitaxy growth, such as solution concentration, deprotonation, temperature and synthesis duration.

4.1.2 Nanometer-level ABBs

The epitaxy growth of nanometer-level ABBs has proven successful in the fabrication of crack-free membranes according to previous reports [91–96]. This process is also termed secondary growth of nanometer-level ABBs as nanoseeds, and illustrates the evolution and ripening of nanometer-level ABBs into bulk and intergrown grains by a solution chemical process. Li et al. demonstrated that ZnO nanoparticles represented an ideal type of nanometer-level ABBs, which could perform as a metal precursors for Zn-based MOF construction [97]. First, the inner wall of the porous alumina tube was coated by a layer of nanoparticle ZnO ABBs with an ultrathin cover of GO nanosheets. Then, GO-guided epitaxy growth of metal oxide as nanometer-level ABBs into crack-free oriented membranes was achieved through a solverthermal process (Fig. 11(a)). The synthesized membrane showed H_2 permeance of 1.5×10^{-7} $mol \cdot m^{-2} \cdot s^{-1} \cdot Pa^{-1}$ and H_2/CO_2 ideal selectivity of 106. Recently, Sun et al. developed an air-liquid interface-assisted deposition method to assemble NH_2-MIL-125 (Ti) nanocrystals on the porous alumina substrate surface, with the aim of forming tight packed and *c*-oriented monolayers of nanometer-level ABBs (Fig. 11(b)) [98]. The epitaxy growth of ABBs was achieved in a synthesis solution composed of TiS_2 (metal

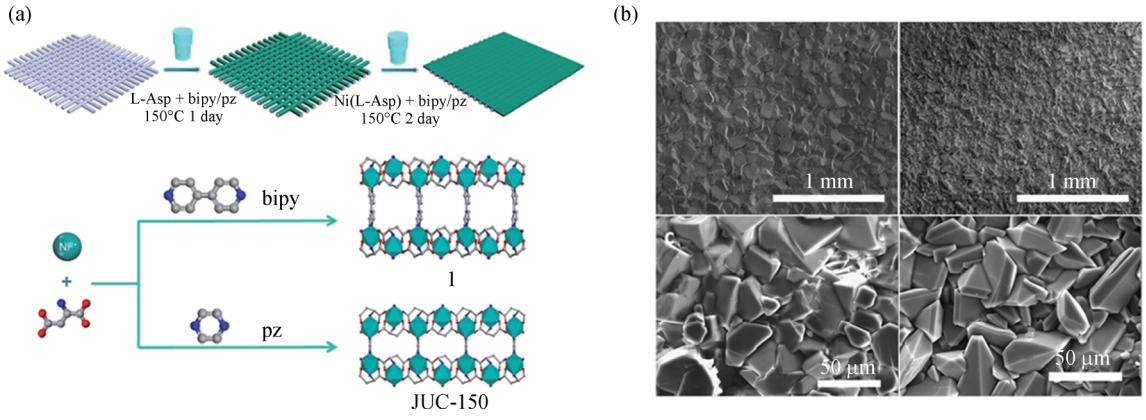

Fig. 10 (a) Schematic diagram of the preparation of $Ni_2(L\text{-}Asp)_2P$ (P = bipy or pz) membranes on nickel screens. Ni, cyan; C, gray; N, blue; O, red; the H atoms are omitted for clarity. (b) Large-area top-view SEM images of compound 1 and JUC-150 membranes showed on the left. Reproduced with permission [83], copyright 2014, The Royal Society of Chemistry.

ions) and terephthalic acid (linker) with the assistance of single-mode microwave heating, which led to the formation of a selective, oriented and crack-free MIL-125 membrane. The membrane showed a remarkable separation performance with H_2 permeance of 129.32 GPU and H_2/CO_2 separation factor of 24.8. Sun's work illustrated the evolution from nanometer-level MIL-125 to crack-free oriented MIL-125 membranes, namely *iso*-structural epitaxy growth of nanometer-level ABBs. Another typical example, reported by Kwon and co-workers, illustrated the epitaxy growth of ZIF-8 as nanometer-level ABBs into well-intergrown ZIF-67 membranes, where ZIF-67 has an analogous topological structure to ZIF-8 with the exception of metal nodes [99]. In contrast, Yang and coworkers reported another fascinating process, that is, hetero-structural epitaxy growth based on nanometer-level ABBs. They found that the mono-ligand ZIF-108 featured SOD topological structure can transform into dual-ligand novel structures (i.e., ZIF-78 with GME structure and ZIF-74 with GIS structure) in mild conditions via a ligand exchange process, in which ZIF-108 as nanometer-level ABBs provided sufficient active sites for coordination of novel linkers and embodied suitable secondary building blocks for the regrowth of novel structures (Fig. 12(a)). Based on these results, ZIF-108 as ABBs was plugged into the hierarchically ordered voids of the stainless-steel-mesh support by hand scrubbing, and successively implementing the hetero-structural epitaxy evolution of ZIF-108 into the compact oriented ZIF-78 film (Fig. 12(b)) [49]. This work proved epitaxy growth between hetero-structural MOFs, and showed the possibility from one type of ABBs to membranes with diversified chemical compositions and structures. The crystallinity, size, morphology and coating parameters of nanometer-level ABBs could influence the as-prepared membranes significantly. The competitive evolution of the crystal faces of ABBs always occurs with expitaxy growth, which could produce membranes with a preferred orientation.

4.1.3 Micrometer-level ABBs

Compared with nanometer-level ABBs, micrometer-level ABBs are prone to formation of a bulk film layer on the substrate surface. The epitaxy growth of micrometer-level ABBs into target crack-free membranes is facilitated by solvothermal processes, which is exemplified with layered double hydroxide (LDH) to ZIF-8 epitaxy evolution reported by Liu et al. As shown in Fig. 13(a), a compact $ZnAl\text{-}NO_3$ film as micrometer level ABBs was firstly prepared on an alumina support and then immersed into a linker solution (2-methylimidazole/methanol) [17]. In this process, the epitaxy growth was concomitant with a notable consumption and self-sacrifice of LDH ABBs, which was manifested by a thickness reduction of the LDH layer observed from cross-sectional SEM images. Thanks to the epitaxy growth, a well-intergrown ZIF-8 membrane layer was attached firmly to the LDH bulk layer. The separation factor of mixed CO_2/CH_4 was 12.9, which exceeded the Knudsen value (0.6).

COFs are a new type of porous materials that were established on strong covalent bonds between light elements (C, B, N, O, Si, etc.). COFs feature a flexible skeleton structure, large surface areas and a tunable cavity size [100]. If we consider the "organic" similarity between COFs and MOFs, a bulk layer of COFs has been anticipated as ABBs for the growth of continuous MOF membranes. Fu et al. deposited COF-300 film on polypropylene cyanide (PAN) modified SiO_2 substrate. The film was immersed into a homogenous solution consisting of metal ions and organic linkers to synthesize $Zn_2(bdc)_2(dabco)$. In solution, COF-300 provided amine groups as active points to anchor to the organic linkers and metal ions separately by means of hydrogen bonds and electrostatic forces, which facilitated the incubation of crack-free membranes based on the epitaxy growth of COF as micrometer-level ABBs (Fig. 13(b)) [101].

Besides the solvothermal process, ligand-vapor treat-

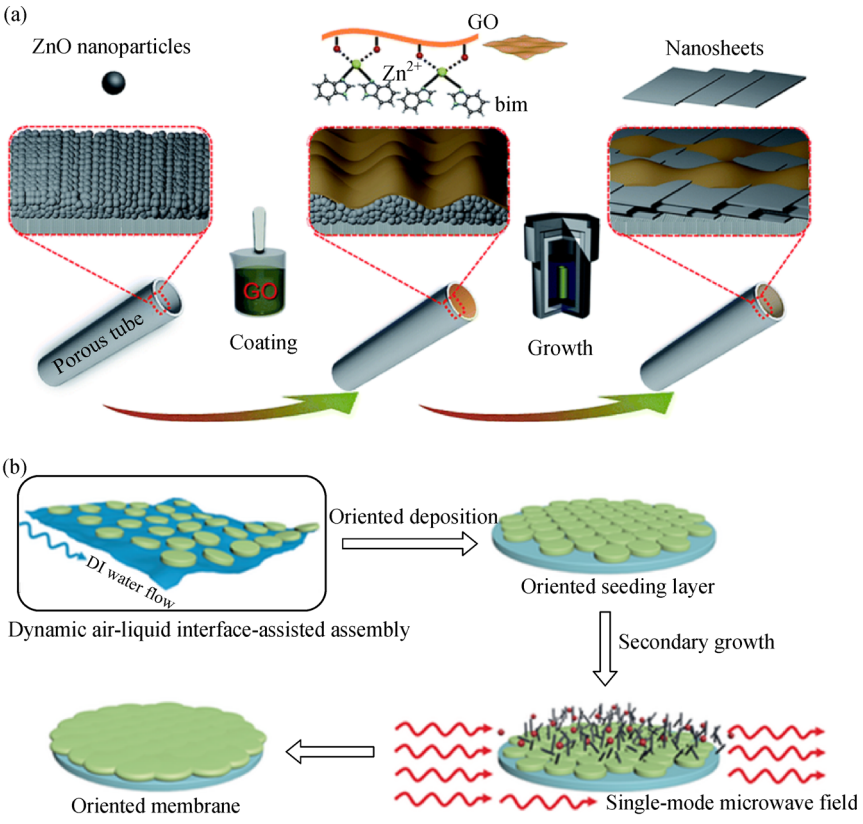

Fig. 11 (a) Schematic illustration of the preparation procedure of highly oriented $Zn_2(bim)_4$ nanosheet membranes by epitaxy growth of ZnO as nanometer-level ABBs with assistance of GO [97]. Copyright 2018, The Royal Society of Chemistry. (b) Procedure for the preparation of highly c-oriented NH_2-MIL-125 (Ti) membranes by epitaxy growth of NH_2-MIL-125 (Ti) as nanometer-level ABBs (red spheres: Ti^{4+} ions; black rods: NH_2-BDC (H_2BDC = terephthalic acid)) [98]. Copyright 2018, Wiley-VCH.

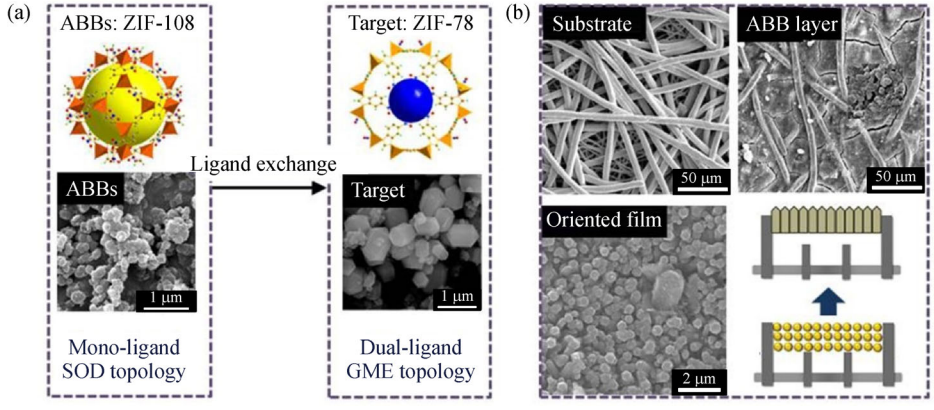

Fig. 12 (a) Synthesis of dual-ligand ZIF-78 with GME topology from mono-ligand ZIF-108 with SOD topology as ABBs; (b) hetero-structural epitaxy growth based on ZIF-108 as nanometer-level ABBs into the oriented ZIF-78 film. Reproduced with permission [49], copyright 2016, Elsevier.

ment also favors the epitaxy growth of micrometer-level ABBs. Ma et al. prepared a dense layer of ZnO in a porous substrate through the chemical vapor deposition method. Followed by ligand-vapor (2-methylimidazole) treatment, the ZnO film as micrometer-level ABBs was transformed partially to ZIF-8 membranes (Fig. 13(c)) [102]. This controlled chemical epitaxy process is suitable for MOF membrane synthesis with satisfied interfacial structures.

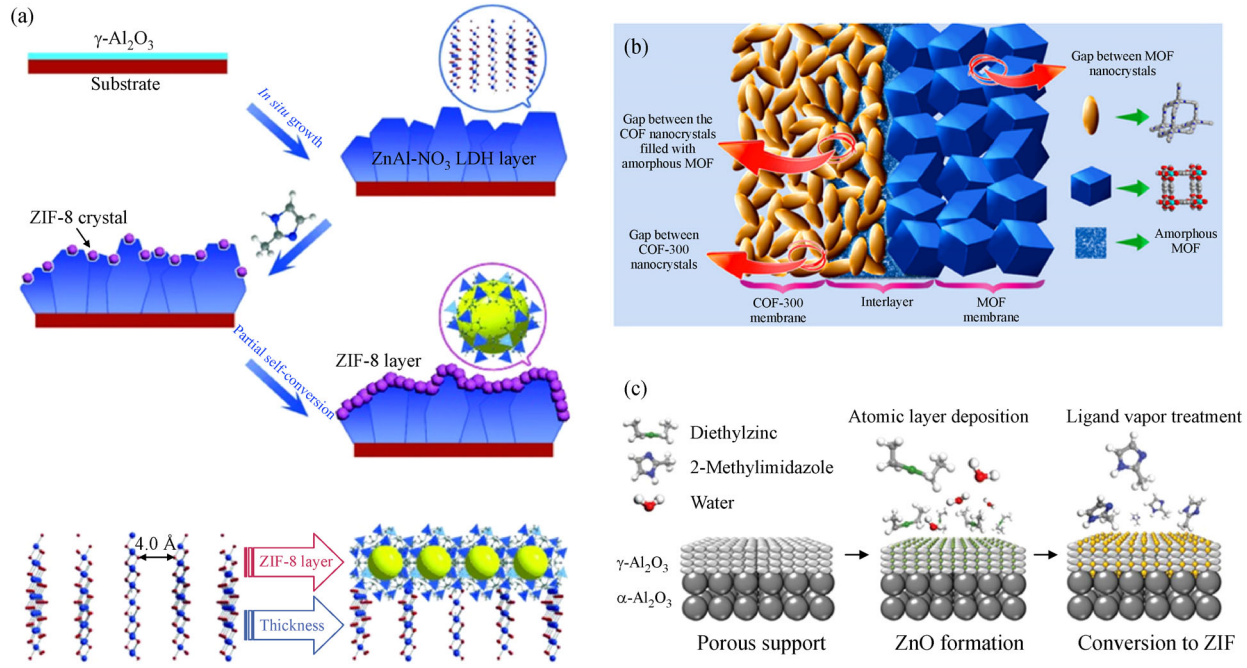

Fig. 13 (a) Epitaxy growth based on LDH as micrometer-level ABBs into ZIF-8 membranes [17]. Copyright 2015, Wiley-VCH. (b) Epitaxy growth based on COF-300 as micrometer-level ABBs into $Zn_2(bdc)_2(dabco)$ membranes [101]. Copyright 2016, American Chemical Society. (c) Epitaxy growth based on ZnO as micrometer-level ABBs into ZIF-8 membrane under ligand-vapor treatment [102]. Copyright 2018, American Association for the Advancement of Science.

The obtained crack-free ZIF-8 membranes exhibited a precise molecular discrimination for the separation of similarly sized gas molecules (e.g., propylene/propane).

The construction of crack-free MOF membranes through chemical epitaxy growth of multiscale-level ABBs has been studied extensively in recent years. ABBs in epitaxy growth for membrane fabrication perform as (i) metal sources for bonding with organic linkers, or (ii) active points for anchoring to reactant precursors for MOF crystallization. ABBs also play a template role in epitaxy growth, which determines the evolution habits and orientation of membranes. Thus, the quality of ABBs (reactivity, continuity, uniformity, compactness and robustness) is of great significance to resultant membranes. Zhou et al. proposed electrodeposition to synthesize a dense layer of ABBs. They revealed that the addition of a small current is helpful to prepare high-quality metal oxide/hydroxide ABBs on substrates [85]. The epitaxy growth of multiscale-level ABBs can be facilitated by solvothermal transformation, vapor induction and other novel controlled processes. Ligand-vapor treatment has been expected to scale up the synthesis of crack-free MOF membranes, which could overcome the hurdles that appear commonly in solvothermal processes, for example, cracks brought about by improper post-treatment, massive consumption of solvents, and complicated operation. Recently, novel technologies such as electrochemical transformation [85], microwave heating and irradiation [103,104] have been developed, which provides further opportunities for the fabrication of crack-free MOF membranes by chemical epitaxy growth based on multiscale-level ABBs.

4.2 Interfacial assembly

Interfacial assembly driven by counter-diffusion of two kinds of precursor solutions (commonly metal ion and linker solutions) has been identified as a feasible way for synthesizing crack-free MOF membranes. Crystallization occurs from the interface to inside a porous substrate where precursors meet, which shows the firm attachment of the MOF membrane to the substrate. With membrane growth, the diffusion of precursor solution in opposite directions occurs through gaps between crystals until a dense and crack-free membrane emerges, which presents the feature of self-termination [18,105–109]. Nair and co-workers proposed a creative interfacial assembly method coupled with microfluidic processing, in which ZIF-8 membranes formed in an oil/water soft interface that was confined by hollow fiber substrates. In this process, two immiscible solvents that contained metal salt and organic ligand flowed on the bore or shell side of the Torlon hollow fiber, respectively (Fig. 14) [110]. The ZIF-8 membrane was formed inside or outside of the fiber surface through a diffusion-driven interfacial assembly process. Amazingly,

membrane growth was highly controlled by varying the microfluidic conditions (continuous bore solution flow, static bore solution and continuous-static intermittent bore solution flow conditions). In the static condition, insufficient Zn^{2+} species were available in the narrow cavity of the hollow fiber, which caused noncontinuous ZIF-8 coatings in the fiber bore. Conversely, continuous flow could favor the rapid diffusion of reactants in opposite directions, which produces a thin membrane layer. Under intermittent conditions, highly intergrown ZIF-8 membranes with different thicknesses were formed. The membrane position (inner surface, outer surface, or in the bulk of the fiber) was finely tuned by the precursor and solvent locations.

The interfacial assembly illustrates a successful approach to synthesizing high-quality crack-free MOF membranes, which relies on the smart design and establishment of well-matched relationships between the nucleation and diffusion via the fine-tuning of synthesis conditions [111]. Membrane assembly in the natural oil/water interface of two kinds of immiscible solvents that contain reactants and precursors is promising. An adjustment of the differences in solubility product constants of two solvents is expected to control the nucleation and subsequent growth of MOF grains and promote the crack-free membrane formation. It is worth noting that the use of novel technology, exemplified with microfluidic processing and microwave heating, plays a key role in balancing the rates of nucleation/crystallization and diffusion for the fabrication of highly crack-free membranes.

4.3 Ultrathin 2D nanosheet assembly

Ultrathin 2D MOF nanosheets with large lateral areas and small thicknesses have been anticipated to be the most appropriate building blocks for ultrathin crack-free MOF membranes with minimization of mass transportation resistance and ultra-permeability in separation. Yang's group carried out pioneering work in the construction of ultrathin MOF membranes based on the assembly of 2D nanosheets [112]. As shown in Fig. 15, a soft-physical process has been developed to exfoliate laminating structure $Zn_2(bim)_4$ (bim = benzimidazole). $Zn_2(bim)_4$ crystals were first wet ball-milled at very low speed followed by exfoliation in volatile solvent with the aid of ultrasonication, to produce one-layer-thick nanosheets (~1 nm) with an intact morphology and ordered structure. A hot-drop coating process was explored to assemble ultrathin MOF membranes with a disordered stacking structure (Fig. 16). With careful optimization, they found that the obtained membranes displayed a proportional correlation between H_2 permeance and H_2/CO_2 separation selectivity (Fig. 16(e)), which was associated closely with the different transportation pathways for H_2 and CO_2. H_2 molecules passed through the flexible aperture window of a lay unit, while CO_2 was detained and transferred slowly through the gaps between layers. By careful optimization, the ultrathin membranes displayed outstanding performances for H_2/CO_2 separation, which far exceeded the latest Robeson's upper-bound for the H_2/CO_2 gas pair.

Recently, Yang's group extended the above strategy to

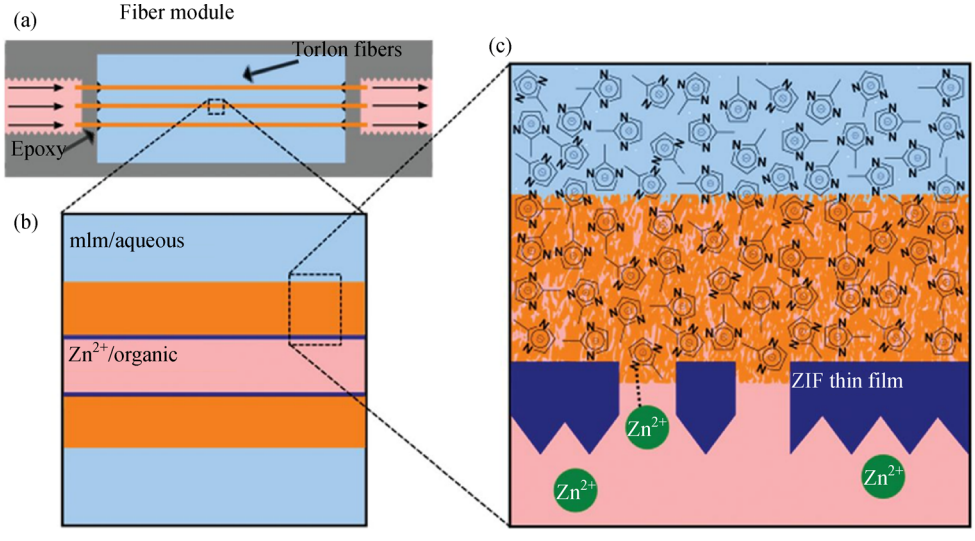

Fig. 14 Scheme depicting the interfacial assembly method coupling with microfluidic processing for MOF membranes in hollow fibers. (a) Side view of a series of fibers mounted in designed reactor. (b) The Zn^{2+} ions are supplied in a 1-octanol solution (light red) flowing through the bore of the fiber, whereas the methylimidazole linkers are supplied on the outer (shell) side of the fiber in an aqueous solution (light blue). (c) Magnified view of fiber support during synthesis. In this example, the membrane forms on the inner surface of the fiber by reaction of the two precursors to form a polycrystalline ZIF-8 layer (dark blue) [110]. Copyright 2014, American Association for the Advancement of Science.

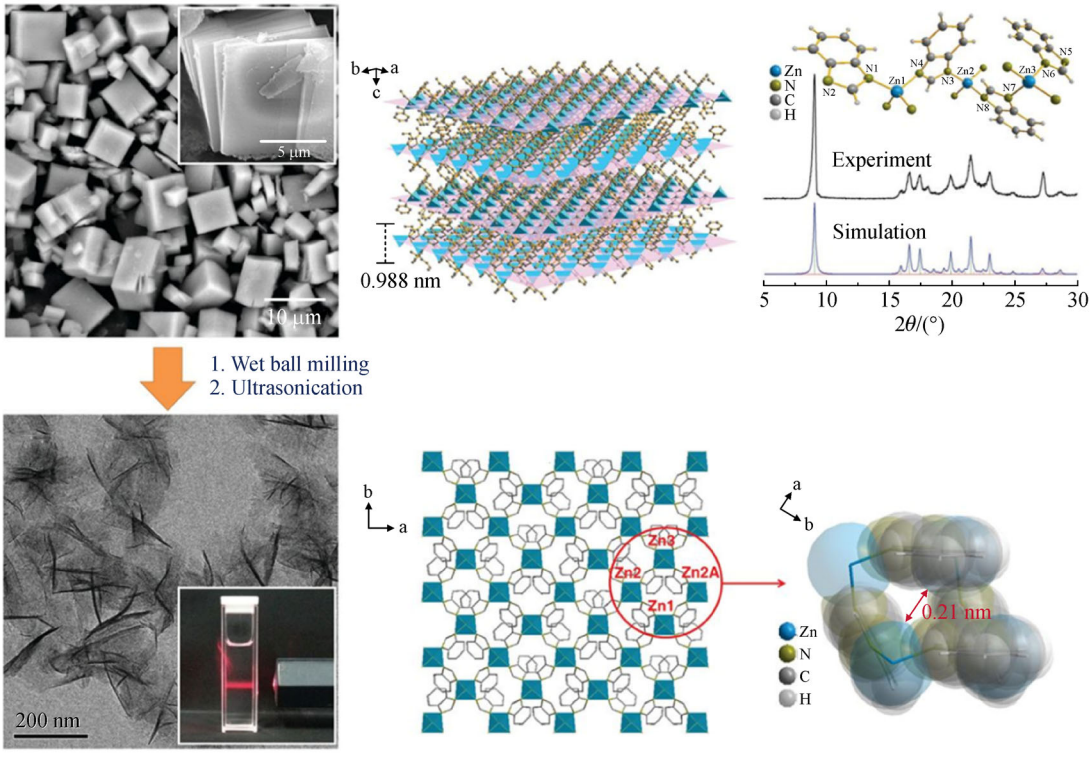

Fig. 15 Top-down fabrication of MOF nanosheets [112]. Copyright 2014, American Association for the Advancement of Science.

synthesize $Zn_2(bim)_3$ crack-free ultrathin membranes [19]. Laminated precursor $Zn_2(bim)_3$ has a double-layered structure stacking in the AB mode. In one layer unit, Zn^{2+} acts as metallic nodes, each of which is connected by three benzimidazole ligands and is saturated by H_2O molecules to form a six-membered-ring pore opening-like structure (Figs. 17(a–c)). The ultrathin membrane assembly of 2D nanosheets revealed an exceptional H_2/CO_2 separation performance. They also found that increasing the temperature could boost the H_2/CO_2 separation performance of the $Zn_2(bim)_3$ ultrathin membrane (Fig. 17(d)), which made it an appropriate candidate for industrial pre-combustion CO_2 capture.

The 2D nanosheet assembly method, which involves laminar exfoliation and post-stacking, is very promising for synthesizing crack-free ultrathin membranes. A perfectly interlocked and close-packed structure between nanosheets is required, which relies highly on the meticulous design of the assembly process and exhaustive structure-performance experiments. The ability to firm the stacking of nanosheets by chemical cross-linkage while maintaining molecular sieving pathways is key to obtain highly crack-free ultrathin nanosheet membranes. Ultrathin membranes based on the perfect assembly of nanosheets have been anticipated to improve the performance benchmark for future CO_2 capture and separation. Chemical/cavity structural design and modification is indispensable to establish a well-matched host-guest relationship for precise sieving.

4.4 Mixed matrix integration

Polymers and ionic liquids are prone to form membranes on substrates because of their flexibility, ductility and processability. If we consider the “prone-to-membrane” feature of polymers and ionic liquids, the mixed matrix approach has been proposed by the rational integration of polymers or ionic liquids (matrix) with MOFs (the second phase) to seal the gaps between MOF crystals elegantly and produce continuous and crack-free hybrid membranes [113–115]. Mixed matrix integration commonly involves three steps, namely membrane solution preparation, membrane coating and post-treatment. Figure 18 shows that compared with traditional inorganic porous materials (e.g., zeolites, carbons and silicas), MOFs as a second phase are more suitable to integrate with polymers and ionic liquids, which avoids significant interphase defects as a result of differences between phases (e.g., thermal expansivity and stiffness/flexibility). This is due to (i) the flexible organic functionalities and exceptional tunability of MOFs that accordingly conduce to the favorable compatibility with polymers and ionic liquids; (ii) easy-to-manipulate crystal size and morphology that permits an ideal dispersion in polymer and ionic liquid matrices. As a

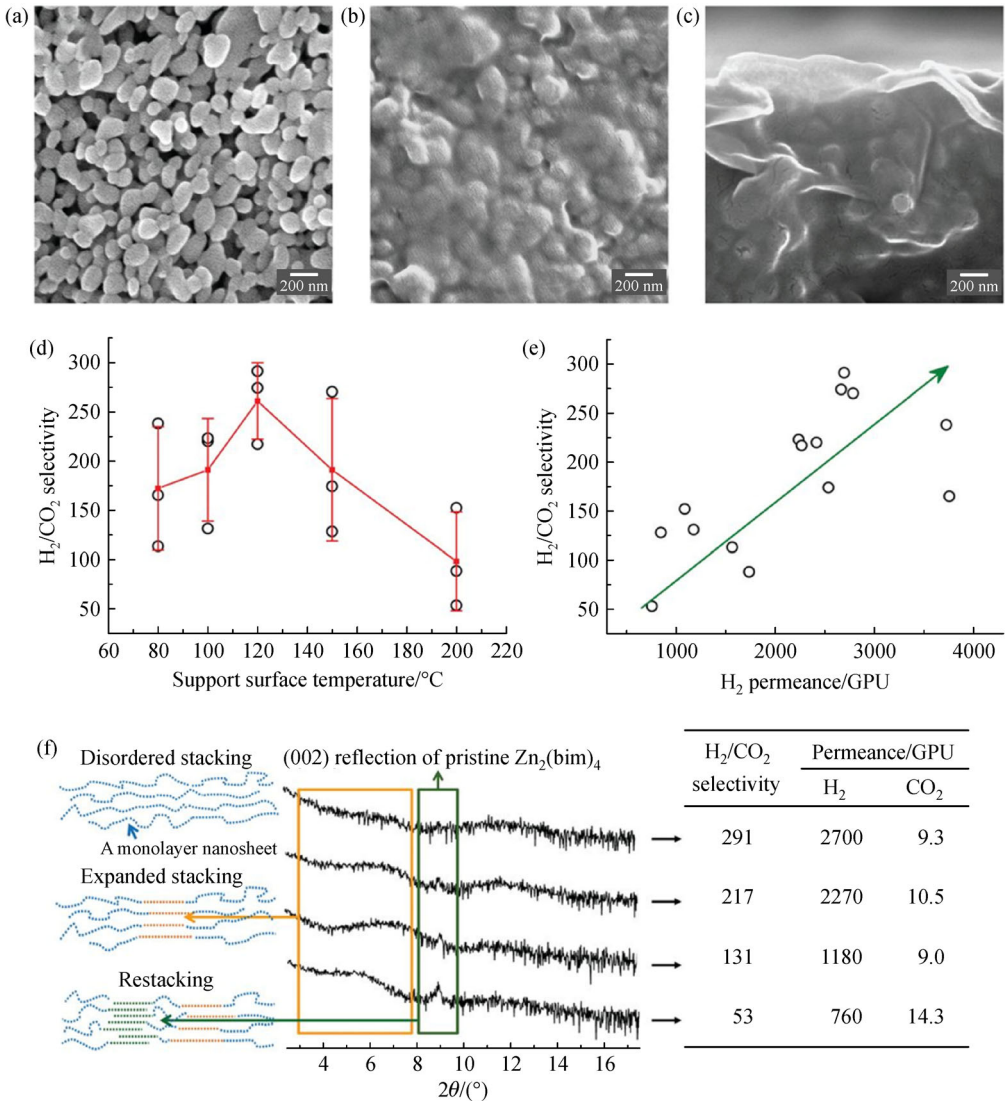

Fig. 16 Morphology and H_2/CO_2 separation performance of ultrathin MOF membranes by nanosheet assembly [112]. Copyright 2014, American Association for the Advancement of Science.

proof-of-concept, various mixed matrix membranes (MMMs) have been designed and synthesized based on MOF crystals [20,116–119].

The interphase structure plays a critical role in the transportation and separation properties of MMMs. Fractional interphase defects may result in crack-flow, which spoils the separation selectivity of MOF-based MMMs. Strengthening interaction between phases means an optimization of the interfacial structure. Essential strategies include (i) optimization of functionalities and crystal size/morphology of MOFs for compatibility and (ii) *in situ* polymerization or crystallization in molecular-level precursor solution for a desirable uniformity and dispersion.

Decorating MOFs with organic functional groups strengthens the interphase interaction between the MOF and the polymer in terms of multiple interaction types (van der Waals force, hydrogen-bonding interaction, covalent bonding interaction, π–π stacking) [120–124]. Zornoza et al. optimized the MOF-polysulfone interactions by using NH_2-modified MIL-53 (Al) as fillers, wherein hydrogen bonding formed between the amine and sulfone groups of both constituents at their interface [124]. Venna et al. grafted various fragments (phenyl acetyl group, decanoyl acetyl group, succinic acid group) on UiO-66. The introduction of UiO-66 decorated with 23 wt-% of phenyl acetyl groups into polyimide matrix led to a 200% increase in CO_2 permeability and 25% increase in CO_2/N_2 selectivity [120]. The exceptional CO_2 separation properties of MMMs are attributed to hydrogen bonds and the π–π stacking force between the modified MOFs and polymer (Fig. 19), which means an intensification of interfacial structures in carefully designed MMMs. The influence of MOF size and morphology on the MMM interface should be considered. Sánchez-Laínez et al.

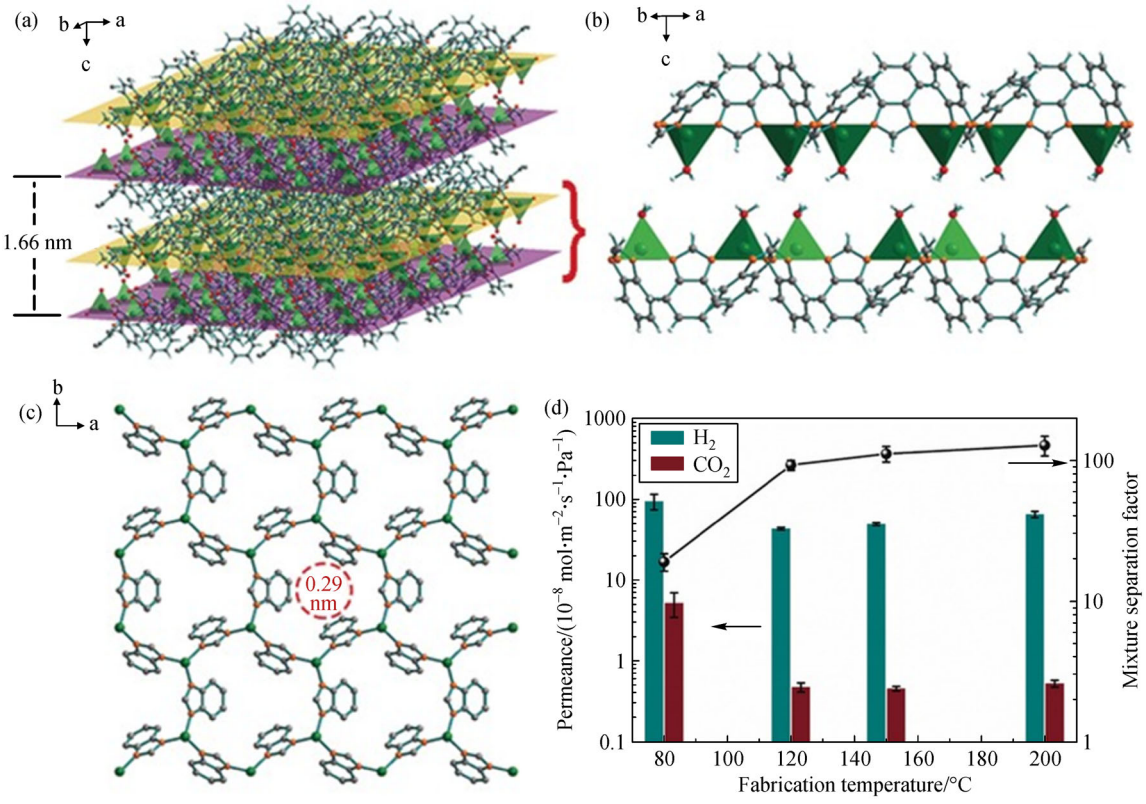

Fig. 17 (a) Four-layered stacking diagram of $Zn_2(bim)_3$ precursors along the *c*-axis. Zn, green; N, orange; C, gray; H, white; O, red. The Zn coordination polyhedra are displayed in green, the layers with benzimidazole ligands along the *c*-axis are depicted in purple, and the others in yellow. (b) Two-layered $Zn_2(bim)_3$ structure highlighting the AB stacking mode. (c) Single-layered nanosheet with the benzo-rings upwards, highlighting the triply-linked coordination of Zn nodes with benzimdazole ligands (H atoms are omitted for clarity). Zn, green; N, orange; C, gray. (d) Binary gas separation performance of equimolar H_2/CO_2 through the $Zn_2(bim)_3$ nanosheet membranes prepared at different temperatures via hot-drop coating method. Reproduced with permission [19], copyright 2017, Wiley-VCH.

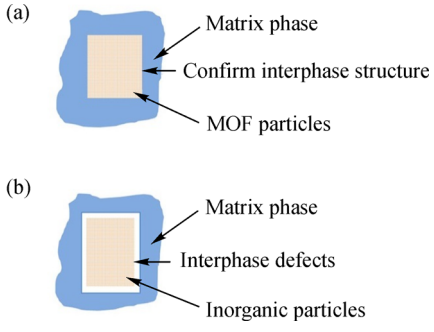

Fig. 18 Illustration of interphase structure of membranes with matrix phase separately integrated with (a) MOF and (b) traditional inorganic particles.

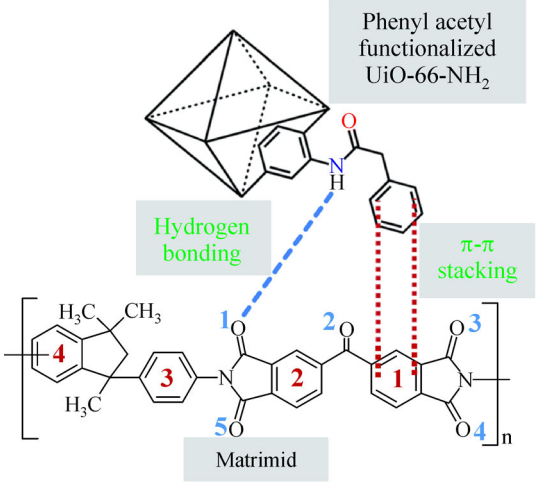

Fig. 19 Scheme demonstrating the favorable interactions between the Matrimid® polymer and modified UiO-66-NH_2 [120]. Copyright 2015, The Royal Society of Chemistry.

reported that ZIF-8 nanoparticles with different sizes (50, 70 and 150 nm) were introduced into the polybenzimidazole (PBI) matrix, where nanoparticles with a grain size of 150 nm represented an optimal choice with the absence of grain aggregation [125]. Sabetghadam et al. studied the effect of filler morphology (nanoparticles, nanorods and microneedles) and showed that MIL nanoparticles favored MMM synthesis with no interfacial cracks, which provided an improved separation performance in CO_2 capture [126].

Rodenas et al. reported that Cu-BDC nanosheet-based MMMs possessed an outstanding CO_2 separation performance, and provided the potential application of MOF lamellae with micrometer lateral dimensions and a nanometer thickness to fabricate crack-free MMMs [118].

In situ polymerization or crystallization in a molecular-level precursor solution favors the uniform dispersion of MOFs in matrices, achieves an ideal compatibility between phases and produces crack-free MMMs. Zhang et al. fabricated high-quality MMMs by *in situ* polymerization of MOFs and monomer solutions [127]. Figure 20(a) shows that nanosized UiO-66-NH_2 was first functionalized with methacrylamide functional groups, and then mixed with butylmethacrylate (BMA) in the presence of the photoinitiator phenylbis (2,4,6-trimethylbenzoyl) phosphine oxide. Exposure to ultraviolet light irradiation for several minutes, MOF-based MMMs with crack-free and uniform structures were obtained. Fan et al. reported the use of a simultaneous spray self-assembly technique to fabricate ZIF-8-polydimethylsiloxane (PDMS) MMMs on polysulfone (PS) substrates [119]. Figure 20(b) shows that the ZIF-8-PDMS suspension and a solution of cross-linking agent tetraethyl orthosilicate (TEOS) and the catalyst dibutyltin dilaurate (DBTDL) were poured separately into two self-stirring pressure barrels and sprayed simultaneously onto a substrate. When the

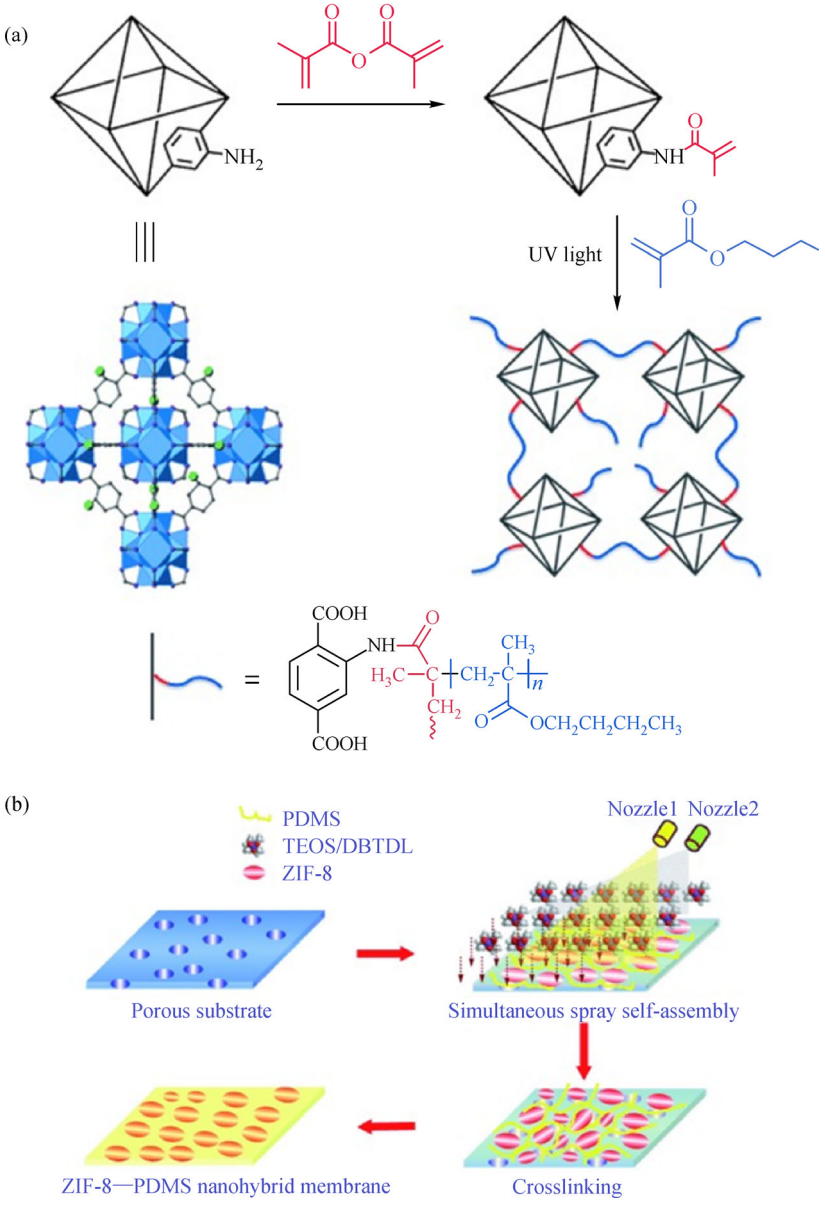

Fig. 20 (a) Post-synthetic modification of UiO-66-NH_2 with methacrylic anhydride and subsequent polymerization with butyl methacrylate (BMA) by irradiation with UV light [127]. Copyright 2015, Wiley-VCH. (b) Formation of the ZIF-8–PDMS nanohybrid composite membrane by the simultaneous spray self-assembly technique [119]. Copyright 2014, Wiley-VCH.

TEOS-DBTDL solution was sprayed, *in situ* cross-linking reactions occurred on the substrate surface. ZIF-8 nanoparticles were surrounded individually by PDMS chains and escaped from aggregation, which ensured the dispersion uniformity of ZIF-8 nanoparticles and the compatibility between phases.

In recent years, mixed matrix integration technology contributed to the preparation of various MOF-based MMMs, providing opportunities for CO_2 capture and separation [14,123,128–130]. Mixed matrix integration represents a smart crack-free membrane concept for CO_2 capture, which inherits and retains the features of MOFs in selective adsorption and transportation. The introduction of well-designed and modified MOFs into matrices (e.g., polymers) significantly improves the CO_2 separation performance. For example, MMMs with amino-decorated UiO-66 displayed an excellent CO_2/N_2 separation performance because of the remarkable affinity of amine groups to CO_2 molecules [131]. Yang and co-workers demonstrated that MMMs that were derived from cage-tailored ZIF-8 nanoparticles exhibited significantly improved molecular sieving properties when splitting CO_2/CH_4 and CO_2/N_2 [14]. They also quantitatively elucidated the contributions of MOF nanoparticles as the second phase in MMMs to adsorption and diffusion parameters [20]. They revealed that MOF nanoparticles dispersed into the polymer matrices built a molecular sieving pathway with a good adsorption affinity to CO_2 molecules, which achieved high-efficiency CO_2/CH_4 separation synergistically. This corroborates that target-oriented design and modification strategies towards chemical/structure factors of MOFs are applicable to construct membranes with high separation performance for CO_2 capture. The development of MMMs with an ultra-high loading of MOFs is needed. Liu et al. proposed the plugging-filling method to synthesize MMMs (Fig. 21) [132]. MOF nanoparticles were firstly plugged into mesh pores of a stainless-steel substrate and gaps between nanoparticles were filled with silicone rubber. By using this method, novel MOF-based MMMs with a high loading ratio (~41.8 wt-%) and an excellent stability were developed. MMMs derived from this strategy have a low cost, processability and robustness, which make them easy-to-commercialize membranes that are suitable for high-efficiency CO_2 separation in the near future.

5 Conclusions and outlook

In recent years, significant progress has been made in MOF-based CO_2 capture. There will be an increasing demand for CO_2-philic materials and, consequently, high-efficiency MOF membranes with a superior permeability and selectivity in the future. Membrane separation is more competitive than adsorption separation in terms of energy consumption. However, the fabrication of crack-free,

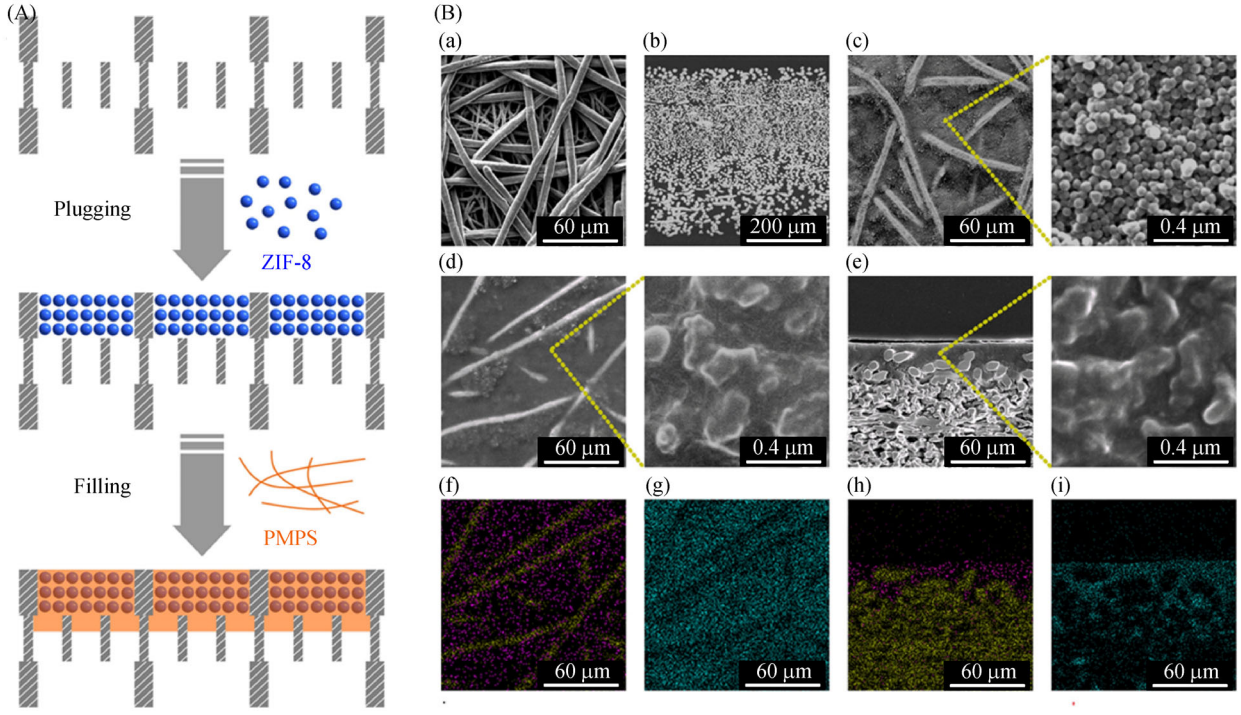

Fig. 21 (A) Schematic illustration of the fabrication procedure of the ZIF-8-PMPS MMMs by the ''plugging-filling'' method. (B) SEM images of (a) top and (b) cross-sectional images of stainless-steel substrate with mesh pores; (c) top images of ZIF-8 nanoparticles plugged into the substrate; (d) top and (e) cross-sectional SEM images of ZIF-8-PMPS MMMs; (f)–(i) EDXS-mappings of (d) and (e) (Zn signal: purple; Fe signal: yellow; Si signal: cyan). Reproduced with permission [132], copyright 2012, Elsevier.

large-area MOF membranes on the industrial scale is still challenging. MOF adsorbents are promising to close the gap between research at the lab scale and practice at the industrial scale for CO_2 capture in a short time. The design and modification of CO_2-philic materials is indispensable. The high degree of control over the chemical and structural features of MOFs is particularly promising, and relies on complete structure-property data chains established from a combination of experiments and computational simulations. Precise design and modification strategies should be stressed, involving (i) secondary building units (metal nodes and linkers) for fine-tuning of the interaction between MOFs and target molecules, to provide sufficient anchoring sites for CO_2 specific adsorption; (ii) architecture (topology and pore structure) that is well-matched with the size and geometry of target molecules, and facilitates CO_2 diffusion and transportation; (iii) hybridization for rational integration of foreign phases, which boosts the selective adsorption and transportation properties.

The construction of crack-free MOF membranes is vitally important to seal the gap between fundamental material design to real-world applications. Two research frontiers of MOF membranes that are suitable for CO_2 capture should be stressed, including (i) ultrathin membranes with a preferential orientation that is based on the systematic engineering of MOF crystal size and morphology to establish optimal transportation pathways for target molecules; (ii) mixed matrix membranes that embody MOF nanoparticles into a continuous matrix phase with a well-designed interfacial structure. These two types of MOF-based membranes have been expected to overcome the permeability-selectivity limitations and reach an economically attractive region. In fact, symmetric MOF-based mixed matrix membranes are still subjected to low permeability compared with pure MOF membranes, which compromises the economic efficiency that arises from the low cost and processability of membranes. This problem could be assessed by using polymeric porous substrates with low capital investment for an asymmetric membrane structure, or by producing membranes in the form of hollow fibers. These endeavors would accelerate the industrialization of MOF-based mixed matrix membranes for real-world CO_2 capture.

In recent years, MOFs have presented additional opportunity for the electrochemical conversion of CO_2 into energy-dense carbon compounds (e.g., CO, methane, methonal) to be used as fuels and chemical feedstock, which highlights a valuable direction for CO_2 used as a source instead of as an emission [133]. Electro-catalytic membrane reactors seem fascinating, and could achieve the simultaneous capture, enrichment and conversion of CO_2 into value-added platform molecules. Outstanding challenges remain in the establishment of systems that feature (i) a highly precise design and modification of CO_2-philic materials with an electro-catalytic activity and a long-term stability; (ii) high-quality membranes with an ultra-high permeability, selectivity and long-term stability to satisfy the demands of electrochemical conversion for the transportation rates and purity of CO_2 feed gas.

Acknowledgements W.Y. thanks the financial support of the Strategic Priority Research Program of the Chinese Academy of Sciences (Grant No. XDB17020400) and the National Natural Science Foundation of China (Grant No. 21721004). Y.B. thanks the financial support of the National Natural Science Foundation of China (Grant No. 21706249) and DICP (Grant No. DICP ZZBS201711).

References

1. Schuur E A G, McGuire A D, Schädel C, Grosse G, Harden J W, Hayes D J, Hugelius G, Koven C D, Kuhry P, Lawrence D M, et al. Climate change and the permafrost carbon feedback. Nature, 2015, 520(7546): 171–179
2. Aghaie M, Rezaei N, Zendehboudi S. A systematic review on CO_2 capture with ionic liquids: Current status and future prospects. Renewable & Sustainable Energy Reviews, 2018, 96: 502–525
3. Trickett C A, Helal A, Al Maythalony B A, Yamani Z H, Cordova K E, Yaghi O M. The chemistry of metal-organic frameworks for CO_2 capture, regeneration and conversion. Nature Reviews Materials, 2017, 2(8): 17045
4. Yu K, Mitch W A, Dai N. Nitrosamines and nitramines in amine-based carbon dioxide capture systems: Fundamentals, engineering implications, and knowledge gaps. Environmental Science & Technology, 2017, 51(20): 11522–11536
5. Huang X, Zhang J, Chen X. $[Zn(bim)_2]\cdot(H_2O)_{1.67}$: A metal-organic open-framework with sodalite topology. Chinese Science Bulletin, 2003, 48(15): 1531–1534
6. Phan A, Doonan C J, Uribe-Romo F J, Knobler C B, O'Keeffe M, Yaghi O M. Synthesis, structure, and carbon dioxide capture properties of zeolitic imidazolate frameworks. Accounts of Chemical Research, 2010, 43(1): 58–67
7. Chui S S Y, Lo S M F, Charmant J P H, Orpen A G, Williams I D. A chemically functionalizable nanoporous material $[Cu_3(TMA)_2(H_2O)_3]_n$. Science, 1999, 283(5405): 1148–1150
8. Mohamed E, Jaheon K, Nathaniel R, David V, Joseph W, Michael O K, Yaghi O M. Systematic design of pore size and functionality in isoreticular MOFs and their application in methane storage. Science, 2002, 295(5554): 469–472
9. Millange F, Serre C, Férey G. Synthesis, structure determination and properties of MIL-53as and MIL-53ht: the first Cr^{III} hybrid inorganic-organic microporous solids: $Cr^{III}(OH)\cdot\{O_2C\text{-}C_6H_4\text{-}CO_2\}\cdot\{HO_2C\text{-}C_6H_4\text{-}CO_2H\}_x$. Chemical Communications, 2002, 8(8): 822–823
10. Cavka J H, Jakobsen S, Olsbye U, Guillou N, Lamberti C, Bordiga S, Lillerud K P. A new zirconium inorganic building brick forming metal organic frameworks with exceptional stability. Journal of the American Chemical Society, 2008, 130(42): 13850–13851
11. Reinsch H, van der Veen M A, Gil B, Marszalek B, Verbiest B, de Vos D, Stock N. Structures, sorption characteristics, and nonlinear optical properties of a new series of highly stable aluminum MOFs.

Chemistry of Materials, 2013, 25(1): 17–26
12. Sholl D S, Lively R P. Seven chemical separations to change the world. Nature, 2016, 532(7600): 435–437
13. Fracaroli A M, Furukawa H, Suzuki M, Dodd M, Okajima S, Gándara F, Reimer J A, Yaghi O M. Metal-organic frameworks with precisely designed interior for carbon dioxide capture in the presence of water. Journal of the American Chemical Society, 2014, 136(25): 8863–8866
14. Ban Y, Li Z, Li Y, Peng Y, Jin H, Jiao W, Guo A, Wang P, Yang Q, Zhong C, Yang W. Confinement of ionic liquids in nanocages: Tailoring the molecular sieving properties of ZIF-8 for membrane-based CO_2 capture. Angewandte Chemie International Edition, 2015, 54(51): 15483–15487
15. Alezi D, Peedikakkal A M P, Weselinski L J, Guillerm V, Belmabkhout Y, Cairns A J, Chen Z, Wojtas L, Eddaoudi M. Quest for highly connected metal-organic framework platforms: Rare-earth polynuclear clusters versatility meets net topology needs. Journal of the American Chemical Society, 2015, 137(16): 5421–5430
16. Zeeshan M, Nozari V, Yagci M B, Isik T, Unal U, Ortalan V, Keskin S, Uzun A. Core-shell type ionic liquid/metal organic framework composite: An exceptionally high CO_2/CH_4 selectivity. Journal of the American Chemical Society, 2018, 140(32): 10113–10116
17. Liu Y, Pan J H, Wang N, Steinbach F, Liu X, Caro J. Remarkably enhanced gas separation by partial self-conversion of a laminated membrane to metal–organic frameworks. Angewandte Chemie International Edition, 2015, 54(10): 3028–3032
18. Kwon H T, Jeong H K. *In situ* synthesis of thin zeolitic-imidazolate framework ZIF-8 membranes exhibiting exceptionally high propylene/propane separation. Journal of the American Chemical Society, 2013, 135(29): 10763–10768
19. Peng Y, Li Y, Ban Y, Yang W. Two-dimensional metal-organic framework nanosheets for membrane-based gas separation. Angewandte Chemie International Edition, 2017, 56(33): 9757–9761
20. Guo A, Ban Y, Yang K, Yang W. Metal-organic framework-based mixed matrix membranes: Synergetic effect of adsorption and diffusion for CO_2/CH_4 separation. Journal of Membrane Science, 2018, 562: 76–84
21. Li Y, Zhang X, Lan J, Xu P, Sun J. Porous Zn(Bmic)(AT) MOF with abundant amino groups and open metal sites for efficient capture and transformation of CO_2. Inorganic Chemistry, 2019, 58 (20): 13917–13926
22. Abdoli Y, Razavian M, Fatemi S. Bimetallic Ni–Co-based metal–organic framework: An open metal site adsorbent for enhancing CO_2 capture. Applied Organometallic Chemistry, 2019, 33(8): e5004
23. Queen W L, Brown C M, Britt D K, Zajdel P, Hudson M R, Yaghi O M. Site-specific CO_2 adsorption and zero thermal expansion in an anisotropic pore network. Journal of Physical Chemistry C, 2011, 115(50): 24915–24919
24. Strauss I, Mundstock A, Hinrichs D, Himstedt R, Knebel A, Reinhardt C, Dorfs D, Caro J. The interaction of guest molecules with Co-MOF-74: A vis/NIR and raman approach. Angewandte Chemie International Edition, 2018, 57(25): 7434–7439
25. Wong-Ng W, Levin I, Kaduk J A, Espinal L, Wu H. CO_2 capture and positional disorder in Cu_3(1,3,5-benzenetricarboxylate)$_2$: An *in situ* laboratory X-ray powder diffraction study. Journal of Alloys and Compounds, 2016, 656: 200–205
26. Wang Q M, Shen D, Bülow M, Lau M L, Deng S, Fitch F R, Lemcoff N O, Semanscin J. Metallo-organic molecular sieve for gas separation and purification. Microporous and Mesoporous Materials, 2002, 55(2): 217–230
27. Caskey S R, Wong-Foy A G, Matzger A J. Dramatic tuning of carbon dioxide uptake via metal substitution in a coordination polymer with cylindrical pores. Journal of the American Chemical Society, 2008, 130(33): 10870–10871
28. Park J, Kim H, Han S S, Jung Y. Tuning metal-organic frameworks with open-metal sites and its origin for enhancing CO_2 affinity by metal substitution. Journal of Physical Chemistry Letters, 2012, 3(7): 826–829
29. Zhai Q G, Bu X, Mao C, Zhao X, Feng P. Systematic and dramatic tuning on gas sorption performance in heterometallic metal-organic frameworks. Journal of the American Chemical Society, 2016, 138(8): 2524–2527
30. Liao P Q, Zang W X, Zhang J P, Chen X M. Efficient purification of ethene by an ethane-trapping metal-organic framework. Nature Communications, 2015, 6 : 8697
31. Zhou D D, Chen P, Wang C, Wang S S, Du Y, Yan H, Ye Z M, He C T, Huang R K, Mo Z W, Huang N Y, Zhang J P. Intermediate-sized molecular sieving of styrene from larger and smaller analogues. Nature Materials, 2019, 18: 994-998
32. Zhang J P, Chen X M. Exceptional framework flexibility and sorption behavior of a multifunctional porous cuprous triazolate framework. Journal of the American Chemical Society, 2008, 130(18): 6010–6017
33. Liao P Q, Chen H, Zhou D D, Liu S, He C, Rui Z, Ji H, Zhang J, Chen X M. Monodentate hydroxide as a super strong yet reversible active site for CO_2 capture from high-humidity flue gas. Energy & Environmental Science, 2015, 8(3): 1011-1016
34. Liao P Q, Zhu A X, Zhang W X, Zhang J P, Chen X M. Self-catalysed aerobic oxidization of organic linker in porous crystal for on-demand regulation of sorption behaviours. Nature Communications, 2015, 6: 6350
35. Zhang J P, Chen X M. Crystal engineering of binary metal imidazolate and triazolate frameworks. Chemical Communications, 2006, (16): 1689–1699
36. Qi X L, Lin R B, Chen Q, Lin J B, Zhang J P, Chen X M. A flexible metal azolate framework with drastic luminescence response toward solvent vapors and carbon dioxide. Chemical Science, 2011, 2(11): 2214–2218
37. Huang X C, Lin Y Y, Zhang J P, Chen X M. Ligand-directed strategy for zeolite-type metal-organic frameworks: Zinc(II) imidazolates with unusual zeolitic topologies. Angewandte Chemie International Edition, 2006, 45(10): 1557–1559
38. Wang X J, Li P Z, Chen Y, Zhang Q, Zhang H, Chan X X, Ganguly R, Li Y, Jiang J, Zhao Y. A rationally designed nitrogen-rich metal-organic framework and its exceptionally high CO_2 and H_2 uptake capability. Scientific Report, 2013, 3: 1149
39. Lu Z, Meng F, Du L, Jiang W, Cao H, Duan J, Huang H, He H. A free tetrazolyl decorated metal-organic framework exhibiting high

and selective CO_2 adsorption. Inorganic Chemistry, 2018, 57(22): 14018–14022

40. Qin J S, Du D Y, Li W L, Zhang J P, Li S L, Su Z M, Wang X L, Xu Q, Shao K Z, Lan Y Q. N-rich zeolite-like metal-organic framework with sodalite topology: High CO_2 uptake, selective gas adsorption and efficient drug delivery. Chemical Science (Cambridge), 2012, 3(6): 2114–2118
41. Li B, Zhang Z, Li Y, Yao K, Zhu Y, Deng Z, Yang F, Zhou X, Li G, Wu H, Nijem N, Chabal Y J, Lai Z, Han Y, Shi Z, Feng S, Li J. Enhanced binding affinity, remarkable selectivity, and high capacity of CO_2 by dual functionalization of a rht-type metal-organic framework. Angewandte Chemie International Edition, 2012, 51(6): 1412–1415
42. Luebke R, Eubank J F, Cairns A J, Belmabkhout Y, Wojtas L, Eddaoudi M. The unique rht-MOF platform, ideal for pinpointing the functionalization and CO_2 adsorption relationship. Chemical Communications, 2012, 48(10): 1455–1457
43. An J, Fiorella R P, Geib S J, Rosi N L. Synthesis, structure, assembly, and modulation of the CO_2 adsorption properties of a zinc-adeninate macrocycle. Journal of the American Chemical Society, 2009, 131(24): 8401–8403
44. An J, Geib S J, Rosi N L. Cation-triggered drug release from a porous zinc-adeninate metal-organic framework. Journal of the American Chemical Society, 2009, 131(24): 8376–8377
45. An J, Geib S J, Rosi N L. High and selective CO_2 uptake in a cobalt adeninate metal-organic framework exhibiting pyrimidine- and amino-decorated pores. Journal of the American Chemical Society, 2010, 132(1): 38–39
46. .Banerjee R, Furukawa H, Britt D, Knobler C, O'Keeffe M, Yaghi O M. Control of pore size and functionality in isoreticular zeolitic imidazolate frameworks and their carbon dioxide selective capture properties. Journal of the American Chemical Society, 2009, 131 (11): 3875–3877
47. Forgan R S, Smaldone R A, Gassensmith J J, Furukawa H, Cordes D B, Li Q, Wilmer C E, Botros Y Y, Snurr R Q, Slawin A M Z, Stoddart J F. Nanoporous carbohydrate metal–organic frameworks. Journal of the American Chemical Society, 2012, 134(1): 406–417
48. Seoane B, Castellanos S, Dikhtiarenko A, Kapteijn F, Gascon J. Multi-scale crystal engineering of metal organic frameworks. Coordination Chemistry Reviews, 2016, 307: 147–187
49. Ban Y, Peng Y, Zhang Y, Jin H, Jiao W, Guo A, Wang P, Li Y, Yang W. Dual-ligand zeolitic imidazolate framework crystals and oriented films derived from metastable mono-ligand ZIF-108. Microporous and Mesoporous Materials, 2016, 219: 190–198
50. Li P Z, Wang X J, Tan R H D, Zhang Q, Zou R, Zhao Y. Rationally "clicked" post-modification of a highly stable metal-organic framework and its high improvement on CO_2-selective capture. RSC Advances, 2013, 3(36): 15566–15570
51. Chen C X, Qiu Q F, Cao C C, Pan M, Wang H P, Jiang J J, Wei Z W, Zhu K, Li G, Su C Y. Stepwise engineering of pore environments and enhancement of CO_2/R22 adsorption capacity through dynamic spacer installation and functionality modification. Chemical Communications, 2017, 53(83): 11403–11406
52. Yan Y, Juríček M, Coudert F X, Vermeulen N A, Grunder S, Dailly A, Lewis W, Blake A J, Stoddart J F, Schröder M. Non-interpenetrated metal–organic frameworks based on copper(II) paddlewheel and oligoparaxylene-isophthalate linkers: Synthesis, structure, and gas adsorption. Journal of the American Chemical Society, 2016, 138(10): 3371–3381
53. Yu M H, Zhang P, Feng R, Yao Z Q, Yu Y C, Hu T L, Bu X H. Construction of a multi-cage-based MOF with a unique network for efficient CO_2 capture. ACS Applied Materials & Interfaces, 2017, 9(31): 26177–26183
54. Zhai Q G, Bu X, Mao C, Zhao X, Daemen L, Cheng Y, Ramirez-Cuesta A J, Feng P. An ultra-tunable platform for molecular engineering of high-performance crystalline porous materials. Nature Communications, 2016, 7(1): 13645
55. Zhai Q G, Bu X, Zhao X, Li D S, Feng P. Pore space partition in metal-organic frameworks. Accounts of Chemical Research, 2017, 50(2): 407–417
56. Zhao X, Bu X, Zhai Q G, Tran H, Feng P. Pore space partition by symmetry-matching regulated ligand insertion and dramatic tuning on carbon dioxide uptake. Journal of the American Chemical Society, 2015, 137(4): 1396–1399
57. Schneemann A, Bon V, Schwedler I, Senkovska I, Kaskel S, Fischer R A. Flexible metal-organic frameworks. Chemical Society Reviews, 2014, 43(16): 6062–6096
58. Bourrelly S, Llewellyn P L, Serre C, Millange F, Loiseau T, Férey G. Different adsorption behaviors of methane and carbon dioxide in the isotypic nanoporous metal terephthalates MIL-53 and MIL-47. Journal of the American Chemical Society, 2005, 127(39): 13519–13521
59. Coudert F X, Mellot-Draznieks C, Fuchs A H, Boutin A. Prediction of breathing and gate-opening transitions upon binary mixture adsorption in metal-organic frameworks. Journal of the American Chemical Society, 2009, 131(32): 11329–11331
60. Lan Y Q, Jiang H L, Li S L, Xu Q. Mesoporous metal-organic frameworks with size-tunable cages: Selective CO_2 uptake, encapsulation of Ln^{3+} cations for luminescence, and column-chromatographic dye separation. Advanced Materials, 2011, 23(43): 5015–5020
61. Llewellyn P L, Bourrelly S, Serre C, Vimont A, Daturi M, Hamon L, De Weireld G, Chang J S, Hong D Y, Kyu Hwang Y, Hwa Jhung S, Férey G. High uptakes of CO_2 and CH_4 in mesoporous metal-organic frameworks MIL-100 and MIL-101. Langmuir, 2008, 24(14): 7245–7250
62. Zheng B, Yang Z, Bai J, Li Y, Li S. High and selective CO_2 capture by two mesoporous acylamide-functionalized rht-type metal-organic frameworks. Chemical Communications, 2012, 48(56): 7025–7027
63. Mao Y, Chen D, Hu P, Guo Y, Ying Y, Ying W, Peng X. Hierarchical mesoporous metal-organic frameworks for enhanced CO_2 capture. Chemistry (Weinheim an der Bergstrasse, Germany), 2015, 21(43): 15127–15132
64. Liu D, Zou D, Zhu H, Zhang J. Mesoporous metal-organic frameworks: Synthetic strategies and emerging applications. Small, 2018, 14(37): 1801454
65. Anderson R, Rodgers J, Argueta E, Biong A, Gomez-Gualdron D A. Role of pore chemistry and topology in the CO_2 capture capabilities of MOFs: From molecular simulation to machine learning. Chemistry of Materials, 2018, 30(18): 6325–6337

66. Xue D X, Cairns A J, Belmabkhout Y, Wojtas L, Liu Y, Alkordi M H, Eddaoudi M. Tunable rare-earth fcu-MOFs: A platform for systematic enhancement of CO_2 adsorption energetics and uptake. Journal of the American Chemical Society, 2013, 135(20): 7660–7667
67. Luebke R, Belmabkhout Y, Weseliński Ł J, Cairns A J, Alkordi M, Norton G, Wojtas Ł, Adil K, Eddaoudi M. Versatile rare earth hexanuclear clusters for the design and synthesis of highly-connected ftw-MOFs. Chemical Science (Cambridge), 2015, 6(7): 4095–4102
68. Zhong R, Yu X, Meng W, Liu J, Zhi C, Zou R. Amine-grafted MIL-101(Cr) via double-solvent incorporation for synergistic enhancement of CO_2 uptake and selectivity. ACS Sustainable Chemistry & Engineering, 2018, 6(12): 16493–16502
69. Lin Y, Lin H, Wang H, Suo Y, Li B, Kong C, Chen L. Enhanced selective CO_2 adsorption on polyamine/MIL-101(Cr) composites. Journal of Materials Chemistry A, 2014, 2(35): 14658–14665
70. Kumar R, Raut D, Ramamurty U, Rao C N R. Remarkable improvement in the mechanical properties and CO_2 uptake of MOFs brought about by covalent linking to graphene. Angewandte Chemie International Edition, 2016, 55(27): 7857–7861
71. Ban Y, Li Y, Peng Y, Jin H, Jiao W, Liu X, Yang W. Metal-substituted zeolitic imidazolate framework ZIF-108: Gas-sorption and membrane separation properties. Chemistry (Weinheim an der Bergstrasse, Germany), 2014, 20(36): 11402–11409
72. Cheng Y, Ying Y, Zhai L, Liu G, Dong J, Wang Y, Christopher M P, Long S, Wang Y, Zhao D. Mixed matrix membranes containing MOF@COF hybrid fillers for efficient CO_2/CH_4 separation. Journal of Membrane Science, 2019, 573: 97–106
73. Li F, Wang D, Xing Q J, Zhou G, Liu S S, Li Y, Zheng L L, Ye P, Zou J P. Design and syntheses of MOF/COF hybrid materials via postsynthetic covalent modification: An efficient strategy to boost the visible-light-driven photocatalytic performance. Applied Catalysis B: Environmental, 2019, 243: 621–628
74. Peng Y, Zhao M, Chen B, Zhang Z, Huang Y, Dai F, Lai Z, Cui X, Tan C, Zhang H. Hybridization of MOFs and COFs: A new strategy for construction of MOF@COF core-shell hybrid materials. Advanced Materials, 2018, 30(3): 1705454
75. Zhang F M, Sheng J L, Yang Z D, Sun X J, Tang H L, Lu M, Dong H, Shen F C, Liu J, Lan Y Q. Rational design of MOF/COF hybrid materials for photocatalytic H_2 evolution in the presence of sacrificial electron donors. Angewandte Chemie International Edition, 2018, 57(37): 12106–12110
76. Liao P Q, Huang N Y, Zhang W X, Zhang J P, Chen X M. Controlling guest conformation for efficient purification of butadiene. Science, 2017, 356(6343): 1193–1196
77. He C T, Ye Z M, Xu Y T, Zhou D D, Zhou H L, Chen D, Zhang J P, Chen X M. Hyperfine adjustment of flexible pore-surface pockets enables smart recognition of gas size and quadrupole moment. Chemical Science (Cambridge), 2017, 8(11): 7560–7565
78. Altintas C, Keskin S. Molecular simulations of MOF membranes and performance predictions of MOF/polymer mixed matrix membranes for CO_2/CH_4 separations. ACS Sustainable Chemistry & Engineering, 2019, 7(2): 2739–2750
79. Qiao Z, Peng C, Zhou J, Jiang J. High-throughput computational screening of 137953 metal-organic frameworks for membrane separation of a $CO_2/N_2/CH_4$ mixture. Journal of Materials Chemistry. A, Materials for Energy and Sustainability, 2016, 4(41): 15904–15912
80. Watanabe T, Sholl D S. Accelerating applications of metal–organic frameworks for gas adsorption and separation by computational screening of materials. Langmuir, 2012, 28(40): 14114–14128
81. Chung Y G, Gómez-Gualdrón D A, Li P, Leperi K T, Deria P, Zhang H, Vermeulen N A, Stoddart J F, You F, Hupp J T, Farha O K, Snurr R Q. *In silico* discovery of metal-organic frameworks for precombustion CO_2 capture using a genetic algorithm. Science Advances, 2016, 2(10): e1600909
82. Guo H, Zhu G, Hewitt I J, Qiu S. "Twin copper source" growth of metal-organic gramework membrane: $Cu_3(BTC)_2$ with high permeability and selectivity for recycling H_2. Journal of the American Chemical Society, 2009, 131(5): 1646–1647
83. Kang Z, Xue M, Fan L, Huang L, Guo L, Wei G, Chen B, Qiu S. Highly selective sieving of small gas molecules by using an ultra-microporous metal-organic framework membrane. Energy & Environmental Science, 2014, 7(12): 4053–4060
84. Hu Y, Dong X, Nan J, Jin W, Ren X, Xu N, Lee Y M. Metal-organic framework membranes fabricated via reactive seeding. Chemical Communications, 2011, 47(2): 737–739
85. Zhou S, Wei Y, Zhuang L, Ding L X, Wang H. Introduction of metal precursors by electrodeposition for the *in situ* growth of metal-organic framework membranes on porous metal substrates. Journal of Materials Chemistry. A, Materials for Energy and Sustainability, 2017, 5(5): 1948–1951
86. Huang A, Bux H, Steinbach F, Caro J. Molecular-sieve membrane with hydrogen permselectivity: ZIF-22 in LTA topology prepared with 3-aminopropyltriethoxysilane as covalent linker. Angewandte Chemie International Edition, 2010, 49(29): 4958–4961
87. Huang A, Dou W, Caro J. Steam-stable zeolitic imidazolate framework ZIF-90 membrane with hydrogen selectivity through covalent functionalization. Journal of the American Chemical Society, 2010, 132(44): 15562–15564
88. McCarthy M C, Varela-Guerrero V, Barnett G V, Jeong H K. Synthesis of zeolitic imidazolate framework films and membranes with controlled microstructures. Langmuir, 2010, 26(18): 14636–14641
89. Bétard A, Bux H, Henke S, Zacher D, Caro J, Fischer R A. Fabrication of a CO_2-selective membrane by stepwise liquid-phase deposition of an alkylether functionalized pillared-layered metal-organic framework $[Cu_2L_2P]_n$ on a macroporous support. Microporous and Mesoporous Materials, 2012, 150: 76–82
90. Fan S, Wu S, Liu J, Liu D. Fabrication of MIL-120 membranes supported by α-Al_2O_3 hollow ceramic fibers for H_2 separation. RSC Advances, 2015, 5(67): 54757–54761
91. Bohrman J A, Carreon M A. Synthesis and CO_2/CH_4 separation performance of Bio-MOF-1 membranes. Chemical Communications, 2012, 48(42): 5130–5132
92. Bux H, Feldhoff A, Cravillon J, Wiebcke M, Li Y S, Caro J. Oriented zeolitic imidazolate framework-8 membrane with sharp H_2/C_3H_8 molecular sieve separation. Chemistry of Materials, 2011, 23(8): 2262–2269
93. Dong X, Lin Y S. Synthesis of an organophilic ZIF-71 membrane for pervaporation solvent separation. Chemical Communications,

2013, 49(12): 1196–1198
94. Li Y S, Bux H, Feldhoff A, Li G L, Yang W S, Caro J. Controllable synthesis of metal-organic frameworks: From MOF nanorods to oriented MOF membranes. Advanced Materials, 2010, 22(30): 3322–3326
95. Liu Y, Hu E, Khan E A, Lai Z. Synthesis and characterization of ZIF-69 membranes and separation for CO_2/CO mixture. Journal of Membrane Science, 2010, 353(1): 36–40
96. Mao Y, Cao W, Li J, Liu Y, Ying Y, Sun L, Peng X. Enhanced gas separation through well-intergrown MOF membranes: Seed morphology and crystal growth effects. Journal of Materials Chemistry. A, Materials for Energy and Sustainability, 2013, 1(38): 11711–11716
97. Li Y, Liu H, Wang H, Qiu J, Zhang X. GO-guided direct growth of highly oriented metal organic framework nanosheet membranes for H_2/CO_2 separation. Chemical Science (Cambridge), 2018, 9(17): 4132–4141
98. Sun Y, Liu Y, Caro J, Guo X, Song C, Liu Y. In-plane epitaxial growth of highly c-oriented NH_2-MIL-125(Ti) membranes with superior H_2/CO_2 selectivity. Angewandte Chemie International Edition, 2018, 57(49): 16088–16093
99. Kwon H T, Jeong H K, Lee A S, An H S, Lee J S. Heteroepitaxially grown zeolitic imidazolate framework membranes with unprecedented propylene/propane separation performances. Journal of the American Chemical Society, 2015, 137(38): 12304–12311
100. Feng X, Ding X, Jiang D. Covalent organic frameworks. Chemical Society Reviews, 2012, 41(18): 6010–6022
101. Fu J, Das S, Xing G, Ben T, Valtchev V, Qiu S. Fabrication of COF-MOF composite membranes and their highly selective separation of H_2/CO_2. Journal of the American Chemical Society, 2016, 138(24): 7673–7680
102. Ma X, Kumar P, Mittal N, Khlyustova A, Daoutidis P, Mkhoyan K A, Tsapatsis M. Zeolitic imidazolate framework membranes made by ligand-induced permselectivation. Science, 2018, 361(6406): 1008–1011
103. Li Y, Yang W. Microwave synthesis of zeolite membranes: A review. Journal of Membrane Science, 2008, 316(1): 3–17
104. Bux H, Liang F, Li Y, Cravillon J, Wiebcke M, Caro J. Zeolitic imidazolate framework membrane with molecular sieving properties by microwave-assisted solvothermal synthesis. Journal of the American Chemical Society, 2009, 131(44): 16000–16001
105. Kwona H T, Jeong H K. Improving propylene/propane separation performance of zeolitic-imidazolate framework ZIF-8 membranes. Chemical Engineering Science, 2015, 124: 20–26
106. Yao J, Dong D, Li D, He L, Xu G, Wang H. Contra-diffusion synthesis of ZIF-8 films on a polymer substrate. Chemical Communications, 2011, 47(9): 2559–2561
107. Kwon H T, Jeong H K. Highly propylene-selective supported zeolite-imidazolate framework (ZIF-8) membranes synthesized by rapid microwave-assisted seeding and secondary growth. Chemical Communications, 2013, 49(37): 3854–3856
108. Lee M J, Kwon H T, Jeong H K. High-flux zeolitic imidazolate framework membranes for propylene/propane separation by postsynthetic linker exchange. Angewandte Chemie International Edition, 2018, 57(1): 156–161
109. Barankova E, Tan X, Villalobos L F, Litwiller E, Peinemann K V. A metal chelating porous polymeric support: The missing link for a defect-free metal-organic framework composite membrane. Angewandte Chemie International Edition, 2017, 56(11): 2965–2968
110. Brown A J, Brunelli N A, Eum K, Rashidi F, Johnson J R, Koros W J, Jones C W, Nair S. Interfacial microfluidic processing of metal-organic framework hollow fiber membranes. Science, 2014, 345(6192): 72–75
111. Eum K, Rownaghi A, Choi D, Bhave R R, Jones C W, Nair S. Fluidic processing of high-performance ZIF-8 membranes on polymeric hollow fibers: Mechanistic insights and microstructure control. Advanced Functional Materials, 2016, 26(28): 5011–5018
112. Peng Y, Li Y, Ban Y, Jin H, Jiao W, Liu X, Yang W. Metal-organic framework nanosheets as building blocks for molecular sieving membranes. Science, 2014, 346(6215): 1356–1359
113. Hao L, Li P, Yang T, Chung T S. Room temperature ionic liquid/ZIF-8 mixed-matrix membranes for natural gas sweetening and post-combustion CO_2 capture. Journal of Membrane Science, 2013, 436: 221–231
114. Tzialla O, Veziri C, Papatryfon X, Beltsios K G, Labropoulos A, Iliev B, Adamova G, Schubert T J S, Kroon M C, Francisco M, Zubeir L F, Romanos G E, Karanikolos G N. Zeolite imidazolate framework–ionic liquid hybrid membranes for highly selective CO_2 separation. Journal of Physical Chemistry C, 2013, 117(36): 18434–18440
115. Bara J E, Hatakeyama E S, Gin D L, Noble R D. Improving CO_2 permeability in polymerized room-temperature ionic liquid gas separation membranes through the formation of a solid composite with a room-temperature ionic liquid. Polymers for Advanced Technologies, 2008, 19(10): 1415–1420
116. Aroon M A, Ismail A F, Matsuura T, Montazer-Rahmati M M. Performance studies of mixed matrix membranes for gas separation: A review. Separation and Purification Technology, 2010, 75(3): 229–242
117. Seoane B, Coronas J, Gascon I, Benavides M E, Karvan O, Caro J, Kapteijn F, Gascon J. Metal–organic framework based mixed matrix membranes: A solution for highly efficient CO_2 capture. Chemical Society Reviews, 2015, 44(8): 2421–2454
118. Rodenas T, Luz I, Prieto G, Seoane B, Miro H, Corma A, Kapteijn F, Llabrés i Xamena F X, Gascon J. Metal-organic framework nanosheets in polymer composite materials for gas separation. Nature Materials, 2014, 14(1): 48–55
119. Fan H, Shi Q, Yan H, Ji S, Dong J, Zhang G. Simultaneous spray self-assembly of highly loaded ZIF-8–PDMS nanohybrid membranes exhibiting exceptionally high biobutanol-permselective pervaporation. Angewandte Chemie International Edition, 2014, 53(22): 5578–5582
120. Venna S R, Lartey M, Li T, Spore A, Kumar S, Nulwala H B, Luebke D R, Rosi N L, Albenze E. Fabrication of MMMs with improved gas separation properties using externally-functionalized MOF particles. Journal of Materials Chemistry A, 2015, 3(9): 5014–5022
121. Anjum M W, Vermoortele F, Khan A L, Bueken B, De Vos D E, Vankelecom I F J. Modulated UiO-66-based mixed-matrix membranes for CO_2 separation. ACS Applied Materials & Interfaces, 2015, 7(45): 25193–25201
122. Nik O G, Chen X Y, Kaliaguine S. Functionalized metal organic

framework-polyimide mixed matrix membranes for CO_2/CH_4 separation. Journal of Membrane Science, 2012, 413: 48–61

123. Yang T, Xiao Y, Chung T S. Poly-/metal-benzimidazole nano-composite membranes for hydrogen purification. Energy & Environmental Science, 2011, 4(10): 4171–4180
124. Zornoza B, Martinez-Joaristi A, Serra-Crespo P, Tellez C, Coronas J, Gascon J, Kapteijn F. Functionalized flexible MOFs as fillers in mixed matrix membranes for highly selective separation of CO_2 from CH_4 at elevated pressures. Chemical Communications, 2011, 47(33): 9522–9524
125. Sánchez-Laínez J, Zornoza B, Friebe S, Caro J, Cao S, Sabetghadam A, Seoane B, Gascon J, Kapteijn F, Le Guillouzer C, Clet G, Daturi M, Téllez C, Coronas J. Influence of ZIF-8 particle size in the performance of polybenzimidazole mixed matrix membranes for pre-combustion CO_2 capture and its validation through interlaboratory test. Journal of Membrane Science, 2016, 515: 45–53
126. Sabetghadam A, Seoane B, Keskin D, Duim N, Rodenas T, Shahid S, Sorribas S, Guillouzer C L, Clet G, Tellez C, Daturi M, Coronas J, Kapteijn F, Gascon J. Metal organic framework crystals in mixed-matrix membranes: Impact of the filler morphology on the gas separation performance. Advanced Functional Materials, 2016, 26(18): 3154–3163
127. Zhang Y, Feng X, Li H, Chen Y, Zhao J, Wang S, Wang L, Wang B. Photoinduced postsynthetic polymerization of a metal-organic framework toward a flexible stand-alone membrane. Angewandte Chemie International Edition, 2015, 127(14): 4333–4337
128. Bae T H, Lee J S, Qiu W, Koros W J, Jones C W, Nair S. A high-performance gas-separation membrane containing submicrometer-sized metal–organic framework crystals. Angewandte Chemie International Edition, 2010, 49(51): 9863–9866
129. Ordoñez M J C, Balkus K J Jr, Ferraris J P, Musselman I H. Molecular sieving realized with ZIF-8/Matrimid® mixed-matrix membranes. Journal of Membrane Science, 2010, 361(1): 28–37
130. Yang T, Chung T S. High performance ZIF-8/PBI nano-composite membranes for high temperature hydrogen separation consisting of carbon monoxide and water vapor. International Journal of Hydrogen Energy, 2013, 38(1): 229–239
131. Shen J, Liu G, Huang K, Li Q, Guan K, Li Y, Jin W. UiO-66-polyether block amide mixed matrix membranes for CO_2 separation. Journal of Membrane Science, 2016, 513: 155–165
132. Liu X, Jin H, Li Y, Bux H, Hu Z, Ban Y, Yang W. Metal-organic framework ZIF-8 nanocomposite membrane for efficient recovery of furfural via pervaporation and vapor permeation. Journal of Membrane Science, 2013, 428: 498–506
133. Kornienko N, Zhao Y, Kley C S, Zhu C, Kim D, Lin S, Chang C J, Yaghi O M, Yang P. Metal-organic frameworks for electrocatalytic reduction of carbon dioxide. Journal of the American Chemical Society, 2015, 137(44): 14129–14135